



HAL
open science

Mellin-Barnes Approach to Hadronic Vacuum Polarization and $g_{\mu-2}$

Jérôme Charles, David Greynat, Eduardo de Rafael

► **To cite this version:**

Jérôme Charles, David Greynat, Eduardo de Rafael. Mellin-Barnes Approach to Hadronic Vacuum Polarization and $g_{\mu-2}$. *Physical Review D*, 2018, 97 (7), pp.076014. 10.1103/PhysRevD.97.076014 . hal-01658449

HAL Id: hal-01658449

<https://hal.science/hal-01658449>

Submitted on 23 Apr 2018

HAL is a multi-disciplinary open access archive for the deposit and dissemination of scientific research documents, whether they are published or not. The documents may come from teaching and research institutions in France or abroad, or from public or private research centers.

L'archive ouverte pluridisciplinaire **HAL**, est destinée au dépôt et à la diffusion de documents scientifiques de niveau recherche, publiés ou non, émanant des établissements d'enseignement et de recherche français ou étrangers, des laboratoires publics ou privés.

The Mellin-Barnes Approach to Hadronic Vacuum Polarization and $g_\mu - 2$

Jérôme Charles¹, David Greynat², Eduardo de Rafael¹

¹ *Aix-Marseille Univ, Université de Toulon, CNRS, CPT, Marseille, France*

² *No affiliation*

Abstract

It is shown that with a precise determination of a few derivatives of the hadronic vacuum polarization (HVP) self-energy function $\Pi(Q^2)$ at $Q^2 = 0$, from lattice QCD (LQCD) or from a dedicated low-energy experiment, one can obtain an evaluation of the lowest order HVP contribution to the anomalous magnetic moment of the muon a_μ^{HVP} with an accuracy comparable to the one reached using the e^+e^- annihilation cross-section into hadrons. The technique of Mellin-Barnes approximants (MBa) that we propose is illustrated in detail with the example of the two loop vacuum polarization function in QED. We then apply it to the first few moments of the hadronic spectral function obtained from experiment and show that the resulting MBa evaluations of a_μ^{HVP} converge very quickly to the full experimental determination.

I Introduction.

This paper explains and develops the approach recently described by one of the authors in refs. [1, 2, 3] to evaluate the hadronic vacuum polarization (HVP) contribution to the anomalous magnetic moment of the muon a_μ^{HVP} .

Our motivation is threefold:

1. The persistent discrepancy at the $\sim 4\sigma$ level between the experimental determination of the anomalous magnetic moment of the muon [4]

$$a_\mu(\text{E821} - \text{BNL}) = 116\,592\,089(54)_{\text{stat}}(33)_{\text{syst}} \times 10^{-11} [0.54\text{ppm}], \quad (1.1)$$

and the standard model prediction [5]

$$a_\mu(\text{SM}) = 116\,591\,805(42) \times 10^{-11}. \quad (1.2)$$

2. The fact that the standard model contribution which at present has the largest error, is the one coming from the lowest order hadronic vacuum polarization (HVP) contribution to $a_\mu(\text{SM})$, evaluated from a combination of experimental results on e^+e^- data [6, 7, 8, 9]:

$$a_\mu^{\text{HVP}} = (6.931 \pm 0.034) \times 10^{-8} [8] \quad \text{and} \quad a_\mu^{\text{HVP}} = (6.933 \pm 0.025) \times 10^{-8} [9]. \quad (1.3)$$

3. The possibility of an alternative evaluation of a_μ^{HVP} , either based on QCD first principles with the help of lattice QCD (LQCD) simulations (see e.g. refs. [10] to [19]), or on new dedicated experiments as proposed in ref. [20].

The standard representation of a_μ^{HVP} used in the experimental determinations is the one in terms of a weighted integral of the hadronic spectral function $\frac{1}{\pi}\text{Im}\Pi(t)$:

$$a_\mu^{\text{HVP}} = \frac{\alpha}{\pi} \int_{4m_\pi^2}^{\infty} \frac{dt}{t} \int_0^1 dx \frac{x^2(1-x)}{x^2 + \frac{t}{m_\mu^2}(1-x)} \frac{1}{\pi} \text{Im}\Pi(t). \quad (1.4)$$

Thanks to the optical theorem, the hadronic spectral function is obtained from the total e^+e^- cross-section into hadrons via one photon annihilation ($m_e \rightarrow 0$)

$$\sigma(t)_{[e^+e^- \rightarrow (\gamma) \rightarrow \text{Hadrons}]} = \frac{4\pi^2\alpha}{t} \frac{1}{\pi} \text{Im}\Pi(t). \quad (1.5)$$

We observe that the integrand in Eq. (1.4) can be rearranged in a way:

$$a_\mu^{\text{HVP}} = \frac{\alpha}{\pi} \int_0^1 dx (1-x) \int_{4m_\pi^2}^{\infty} \frac{dt}{t} \frac{\frac{x^2}{1-x} m_\mu^2}{t + \frac{x^2}{1-x} m_\mu^2} \frac{1}{\pi} \text{Im}\Pi(t), \quad (1.6)$$

which explicitly displays the dispersion relation between the hadronic spectral function and the renormalized hadronic photon self-energy in the euclidean:

$$-\Pi(Q^2) = \int_{4m_\pi^2}^{\infty} \frac{dt}{t} \frac{Q^2}{t + Q^2} \frac{1}{\pi} \text{Im}\Pi(t), \quad \text{with} \quad Q^2 \equiv \frac{x^2}{1-x} m_\mu^2 \geq 0, \quad (1.7)$$

and therefore [21, 22]

$$a_\mu^{\text{HVP}} = -\frac{\alpha}{\pi} \int_0^1 dx (1-x) \Pi\left(\frac{x^2}{1-x} m_\mu^2\right). \quad (1.8)$$

Trading the Feynman parameter x -integration by a Q^2 -integration results in a slightly more complicated expression

$$a_\mu^{\text{HVP}} = \frac{\alpha}{\pi} \int_0^\infty \frac{dQ^2}{Q^2} \sqrt{\frac{Q^2}{4m_\mu^2 + Q^2}} \left(\frac{\sqrt{4m_\mu^2 + Q^2} - \sqrt{Q^2}}{\sqrt{4m_\mu^2 + Q^2} + \sqrt{Q^2}} \right)^2 [-\Pi(Q^2)], \quad (1.9)$$

which is the one proposed for LQCD evaluations [23]. Because of the weight function in the integrand of Eq. (1.9), the integral is dominated by the low- Q^2 behaviour of the hadronic self-energy function $\Pi(Q^2)$. The natural question which then arises is: *What is the best way to help LQCD evaluations (see e.g. refs. [10] to [19]), or dedicated experiments [20], to evaluate this integral when only limited information about $\Pi(Q^2)$ at low Q^2 values is available?* The answer that we propose follows the way initiated in ref. [2]. It is based on Mellin-Barnes techniques which we shall describe below and which we shall illustrate with several examples. As we shall see, this is a very powerful method compared to other approaches discussed in the literature (see e.g. refs. [24, 25, 26] and references therein).

The paper has been organized as follows. The next section is an introduction to the QCD properties of the Mellin transform of the HVP spectral function. Section III is dedicated to a few ingredients, which are required to understand and justify the method that we propose. The subsection III.3 is particularly technical since it justifies mathematically the underlying approach and the restriction to the subclass of Marichev-like Mellin approximants given in Eq. (3.30). For those who are just interested in the applications, it can be escaped in a first reading. Section IV illustrates the application of Mellin-Barnes approximants (MBa) to vacuum polarization in QED at the two loop level. Section V tests the advocated technique of MBa with experimental HVP moments. It shows how the successive MBa approach the experimental determination of a_μ^{HVP} . The conclusions with an outlook on future work are given in Section VI. A few technical details have been included in an Appendix.

II The Mellin Transform of the Hadronic Spectral Function.

In QCD the hadronic spectral function is positive and goes asymptotically to a constant (q_i denotes the charge, in electric charge units, of an active quark with flavour i) :

$$\frac{1}{\pi} \text{Im}\Pi(t) \underset{t \rightarrow \infty}{\sim} \left(\frac{\alpha}{\pi} \right) \left(\sum_i q_i^2 \right) \frac{1}{3} N_c [1 + \mathcal{O}(\alpha_s)], \quad (2.1)$$

with perturbative QCD (pQCD) α_s -corrections known up to four loops.

The moment integrals

$$\int_{t_0}^\infty \frac{dt}{t} \left(\frac{t_0}{t} \right)^{1+n} \frac{1}{\pi} \text{Im}\Pi(t), \quad t_0 = 4m_{\pi^\pm}^2, \quad n = 0, 1, 2, \dots, \quad (2.2)$$

are therefore well defined and the dispersion relation in Eq. (1.7) relates them to successive derivatives of the hadronic self-energy function $\Pi(Q^2)$ at the origin:

$$\int_{t_0}^\infty \frac{dt}{t} \left(\frac{t_0}{t} \right)^{1+n} \frac{1}{\pi} \text{Im}\Pi(t) = \frac{(-1)^{n+1}}{(n+1)!} (t_0)^{n+1} \left(\frac{\partial^{n+1}}{(\partial Q^2)^{n+1}} \Pi(Q^2) \right)_{Q^2=0}, \quad n = 0, 1, 2, \dots. \quad (2.3)$$

In fact, as pointed out a long time ago [27], the first moment for $n = 0$ provides a rigorous upper bound to the muon anomaly because, going back to Eq. (1.6):

$$\begin{aligned} a_\mu^{\text{HVP}} &= \frac{\alpha}{\pi} \int_{4m_\pi^2}^\infty \frac{dt}{t} \int_0^1 dx \left\{ \frac{x^2(1-x)}{x^2 + \frac{t}{m_\mu^2}(1-x)} < \frac{x^2}{\frac{t}{m_\mu^2}} \right\} \frac{1}{\pi} \text{Im}\Pi(t) \\ &= \frac{\alpha}{\pi} \frac{1}{3} \frac{m_\mu^2}{t_0} \int_{4m_\pi^2}^\infty \frac{dt}{t} \frac{t_0}{t} \frac{1}{\pi} \text{Im}\Pi(t) = \left(\frac{\alpha}{\pi} \right) \frac{1}{3} \frac{m_\mu^2}{t_0} \left(-t_0 \frac{\partial}{\partial Q^2} \Pi(Q^2) \right)_{Q^2=0}. \end{aligned} \quad (2.4)$$

In the case of the anomalous magnetic moment of the electron, because of the small electron mass as compared to hadronic scales, this upper bound gives practically the value of the full contribution

$$a_e^{\text{HVP}} \simeq \frac{\alpha}{\pi} \frac{1}{3} \int_{4m_\pi^2}^{\infty} \frac{dt}{t} \frac{m_e^2}{t} \frac{1}{\pi} \text{Im}\Pi(t). \quad (2.5)$$

The relation

$$\int_{4m_\pi^2}^{\infty} \frac{dt}{t} \frac{1}{t} \frac{1}{\pi} \text{Im}\Pi(t) = \left(-\frac{\partial}{\partial Q^2} \Pi(Q^2) \right)_{Q^2=0}, \quad (2.6)$$

where the l.h.s. is accessible to an experimental determination and the r.h.s. to a LQCD evaluation, provides therefore an excellent comparative test of the two approaches. Quite generally, the moments in Eq. (2.2) obey constraints which follow from the positivity of the spectral function and may provide useful tests to LQCD determinations. We discuss these constraints in the Appendix.

The moment integrals in Eq. (2.2) can be generalized to a function, which is precisely the Mellin transform of the hadronic spectral function $\frac{1}{\pi} \text{Im}\Pi(t)$ defined as follows [1]:

$$\mathcal{M} \left[\frac{1}{\pi} \text{Im}\Pi(t) \right] (s) \equiv \mathcal{M}(s) = \int_{t_0}^{\infty} \frac{dt}{t} \left(\frac{t}{t_0} \right)^{s-1} \frac{1}{\pi} \text{Im}\Pi(t), \quad t_0 = 4m_\pi^2, \quad -\infty \leq \text{Re}(s) < 1, \quad (2.7)$$

where, for practical purposes, we normalize the spectral function t -variable to the two-pion threshold value¹. With this normalization $\mathcal{M}(s)$ is dimensionless and a monotonously increasing function for real s in $]-\infty, 1]$, a fact which follows from the positivity of its derivative in that range:

$$\mathcal{M}'(s) \equiv \frac{d}{ds} \mathcal{M}(s) = \int_{t_0}^{\infty} \frac{dt}{t} \left(\frac{t}{t_0} \right)^{s-1} \log \frac{t}{t_0} \frac{1}{\pi} \text{Im}\Pi(t), \quad -\infty \leq \text{Re}(s) < 1. \quad (2.8)$$

This implies that $\mathcal{M}(s)$ can have neither poles nor zeros in the negative $\text{Re}(s)$ axis.

In QCD, the Mellin transform $\mathcal{M}(s)$ is singular at $s = 1$ with a residue which is fixed by the pQCD asymptotic behaviour of the spectral function in Eq. (2.1). The contribution from the u , d , s , c , b and t quarks gives

$$\mathcal{M}(s) \underset{s \rightarrow 1}{\sim} \left(\frac{\alpha}{\pi} \right) \left(\frac{4}{9} + \frac{1}{9} + \frac{1}{9} + \frac{4}{9} + \frac{1}{9} + \frac{4}{9} \right) N_c \frac{1}{3} \frac{1}{1-s} + \mathcal{O}(\alpha_s). \quad (2.9)$$

The function $\mathcal{M}(s)$ is then defined by the integral in Eq. (2.7) for $\text{Re}(s) < 1$ and extended to the whole complex s -plane by analytic continuation. The spectral function moments are, therefore, the particular values of $\mathcal{M}(s)$ at $s = 0, -1, -2, -N$ with integer N .

As discussed in refs. [1, 2] there exists a representation of $\Pi(Q^2)$, and hence of the anomaly a_μ^{HVP} , in terms of the Mellin transform $\mathcal{M}(s)$. This follows from inserting the Mellin-Barnes identity²

$$\frac{1}{1 + \frac{Q^2}{t}} = \frac{1}{2\pi i} \int_{c_s - i\infty}^{c_s + i\infty} ds \left(\frac{Q^2}{t} \right)^{-s} \Gamma(s) \Gamma(1-s) \quad (2.10)$$

in the dispersion relation in Eq. (1.7), which results in the representation

$$\Pi(Q^2) = -\frac{Q^2}{t_0} \frac{1}{2\pi i} \int_{c_s - i\infty}^{c_s + i\infty} ds \left(\frac{Q^2}{t_0} \right)^{-s} \Gamma(s) \Gamma(1-s) \mathcal{M}(s), \quad c_s \equiv \text{Re}(s) \in]0, 1[. \quad (2.11)$$

¹Notice that in ref. [1] the chosen normalization scale is the muon mass.

²For the benefit of the reader who may be unfamiliar with Mellin-Barnes integrals we give a proof of this identity in the Appendix.

The corresponding integral representation for the Adler function is then

$$\mathcal{A}(Q^2) \equiv -Q^2 \frac{\partial \Pi(Q^2)}{\partial Q^2} = \frac{1}{2\pi i} \int_{c_s - i\infty}^{c_s + i\infty} ds \left(\frac{Q^2}{t_0} \right)^{1-s} \Gamma(s) \Gamma(2-s) \mathcal{M}(s), \quad c_s \equiv \text{Re}(s) \in]0, 1[. \quad (2.12)$$

Setting $Q^2 = \frac{x^2}{1-x} m_\mu^2$ in the representation of $\Pi(Q^2)$ in Eq. (2.11) and inserting it in the r.h.s. of Eq. (1.8) we have

$$a_\mu^{\text{HVP}} = -\frac{\alpha}{\pi} \int_0^1 dx (1-x) \Pi \left(\frac{x^2}{1-x} m_\mu^2 \right) \quad (2.13)$$

$$= \frac{\alpha}{\pi} \int_0^1 dx (1-x) \frac{1}{2\pi i} \int_{c_s - i\infty}^{c_s + i\infty} ds \left(\frac{\frac{x^2}{1-x} m_\mu^2}{t_0} \right)^{1-s} \Gamma(s) \Gamma(1-s) \mathcal{M}(s). \quad (2.14)$$

The integral over the x -parameter can now be made analytically, leading to the expression [1]

$$a_\mu^{\text{HVP}} = \left(\frac{\alpha}{\pi} \right) \frac{m_\mu^2}{t_0} \frac{1}{2\pi i} \int_{c_s - i\infty}^{c_s + i\infty} ds \left(\frac{m_\mu^2}{t_0} \right)^{-s} \mathcal{F}(s) \mathcal{M}(s), \quad c_s \equiv \text{Re}(s) \in]0, 1[, \quad (2.15)$$

where $\mathcal{F}(s)$ is the explicitly known function

$$\mathcal{F}(s) = -\Gamma(3-2s) \Gamma(-3+s) \Gamma(1+s), \quad (2.16)$$

and the hadronic dynamics is entirely factorized in the Mellin transform $\mathcal{M}(s)$.

As discussed in ref. [1] the Mellin-Barnes representation in Eq. (2.15) offers the possibility of computing a_μ^{HVP} as a series expansion in powers of $\frac{m_\mu^2}{t_0}$. This follows from inserting in Eq. (2.15) the *singular expansion* of $\mathcal{F}(s)$ at the l.h.s. of the *fundamental strip* $c_s \equiv \text{Re}(s) \in]0, 1[$ i.e.

$$\mathcal{F}(s) \asymp \frac{1}{3} \frac{1}{s} - \frac{1}{(s+1)^2} + \frac{25}{12} \frac{1}{s+1} - \frac{6}{(s+2)^2} + \frac{97}{10} \frac{1}{s+2} - \frac{28}{(s+3)^2} + \frac{208}{5} \frac{1}{s+3} + \dots, \quad (2.17)$$

and using the *converse mapping theorem* of ref. [28] which relates in a precise way the singularities in the complex s -plane of the integrand in Eq. (2.15) to the successive terms of the $\frac{m_\mu^2}{t_0}$ expansion³. This expansion is governed by the moments $\mathcal{M}(-n)$ at $n = 0, 1, 2, \dots$, and by the $\log \frac{t}{t_0}$ weighted moments $\mathcal{M}'(-n)$ in Eq. (2.8), with the result⁴

$$\begin{aligned} a_\mu^{\text{HVP}} = & \left(\frac{\alpha}{\pi} \right) \frac{m_\mu^2}{t_0} \left\{ \frac{1}{3} \mathcal{M}(0) + \frac{m_\mu^2}{t_0} \left[\left(\frac{25}{12} - \log \frac{t_0}{m_\mu^2} \right) \mathcal{M}(-1) - \mathcal{M}'(-1) \right] \right. \\ & + \left(\frac{m_\mu^2}{t_0} \right)^2 \left[\left(\frac{97}{10} - 6 \log \frac{t_0}{m_\mu^2} \right) \mathcal{M}(-2) - 6 \mathcal{M}'(-2) \right] \\ & \left. + \left(\frac{m_\mu^2}{t_0} \right)^3 \left[\left(\frac{208}{5} - 28 \log \frac{t_0}{m_\mu^2} \right) \mathcal{M}(-3) - 28 \mathcal{M}'(-3) \right] + \mathcal{O} \left(\frac{m_\mu^2}{t_0} \right)^4 \right\}. \quad (2.18) \end{aligned}$$

³See e.g. refs. [29, 30, 31] for applications of the converse mapping theorem in QED.

⁴There are two misprints in the similar Eq. (3.18) in ref. [2]: there should be a factor of 6 in front of $\log \frac{t_0}{m_\mu^2}$ in the second line and a factor 28 in front of $\log \frac{t_0}{m_\mu^2}$ in the third line.

The bulk of the overall contribution to a_μ^{HVP} comes in fact from just the first few terms. The first term is the upper-bound of ref. [27] with successive fast improvements from the following terms. In this paper, however, we shall not follow the idea of performing this $\frac{m_\mu^2}{t_0}$ series expansion evaluation. This is because the direct determination of the $\mathcal{M}'(-n)$ moments in LQCD is not easy. What is required in the case where only the first few moments $\mathcal{M}(-n)$ are known, is a good interpolation method between the moment values which reproduces the contributions from the *a priori unknown* log-weighted moments $\mathcal{M}'(-n)$. This is precisely what the Mellin-Barnes approximants (MBA) method described below do: given N moments $\mathcal{M}(-n)$, $n = 0, 1, \dots, N - 1$, it constructs successive Mellin approximants $\mathcal{M}_N(s)$ to the full Mellin transform $\mathcal{M}(s)$. The approximants $\mathcal{M}_N(s)$ are then inserted in the integrand of the r.h.s. of Eq. (2.15) to evaluate the corresponding $a_\mu^{\text{HVP}}(N)$ result. The numerical integration in Eq. (2.15) being made, for a fixed c_s value within the fundamental strip, along the corresponding imaginary axis.

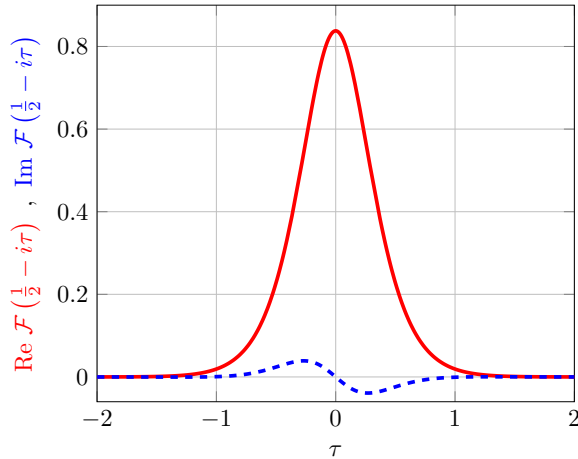


Figure 1:

Shape of the function $\mathcal{F}(\frac{1}{2} - i\tau)$ in Eq. (2.15) versus τ . The red curve is the real part of the function, the blue dashed curve its imaginary part.

The weight function $\mathcal{F}(s)$ in Eq. (2.15) is universal and has a shape which, for the specific choice $s = \frac{1}{2} - i\tau$ is shown in Fig. (1) as a function of τ . Notice that the real part of this function (the red curve) is symmetric under $\tau \rightarrow -\tau$ while its imaginary part is antisymmetric. Both the real and imaginary parts fall very fast as τ increases. With the change of variable

$$s \rightarrow \frac{1}{2} - i\tau, \quad (2.19)$$

the integral in Eq. (2.15) becomes then a Fourier transform:

$$a_\mu^{\text{HVP}} = \left(\frac{\alpha}{\pi}\right) \sqrt{\frac{m_\mu^2}{t_0}} \frac{1}{2\pi} \int_{-\infty}^{+\infty} d\tau e^{i\tau \log \frac{m_\mu^2}{t_0}} \mathcal{F}\left(\frac{1}{2} - i\tau\right) \mathcal{M}\left(\frac{1}{2} - i\tau\right). \quad (2.20)$$

Because of the shape of the $\mathcal{F}(\frac{1}{2} - i\tau)$ function and the growth restrictions on $\mathcal{M}(\frac{1}{2} - i\tau)$ for large τ , which are fixed by the fact that $\Pi(Q^2)$ obeys a dispersion relation in QCD, the Fourier transform above is fully dominated by the behaviour of the integrand in a very restricted τ -interval, $-T \leq \tau \leq +T$ with T of order one.

III Some Technical Ingredients.

We shall next recall a few technical ingredients which in the literature go under the name of: Ramanujan Master Theorem, Marichev class of Mellin transforms, Generalized Hypergeometric Functions and Meijer's G-Functions. They are necessary to implement and justify the MBa framework that we propose.

III.1 The so called Ramanujan's Master Theorem.

Consider a function $F(x)$ which admits a power series expansion

$$F(x) \underset{x \rightarrow 0}{\sim} \lambda(0) - \lambda(-1)x + \lambda(-2)x^2 - \lambda(-3)x^3 + \dots . \quad (3.1)$$

Ramanujan's theorem refers then to the formal identity [32]

$$\int_0^\infty dx x^{s-1} \{ \lambda(0) - \lambda(-1)x + \lambda(-2)x^2 - \lambda(-3)x^3 + \dots \} = \Gamma(s)\Gamma(1-s)\lambda(s), \quad (3.2)$$

and implies that the Mellin transform of $F(x)$ is given by

$$\int_0^\infty dx x^{s-1} F(x) = \Gamma(s)\Gamma(1-s)\lambda(s). \quad (3.3)$$

The function $\lambda(s)$, extended over the full complex s -plane, can be simply obtained from the discrete n -functional dependence of the $\lambda(-n)$ coefficients of the Taylor expansion of $F(x)$ by the formal replacement $n \rightarrow -s$. The proof of this beautiful theorem was provided by Hardy [33] and it is based on Cauchy's residue theorem as well as on the Mellin-Barnes representation. The basic assumption in Hardy's proof is a growth restriction on $|\lambda(s)|$ which assures that the series $\lambda(0) - \lambda(-1)x + \lambda(-2)x^2 - \lambda(-3)x^3 + \dots$ has some radius of convergence. In our case $F(x)$ will be the hadronic photon self-energy function $\Pi(Q^2)$, with $x \equiv \frac{Q^2}{t_0}$, and Hardy's growth restriction is equivalent to the one required to write a dispersion relation for $\Pi(Q^2)$.

At small Q^2 values, the hadronic photon self-energy function $\Pi(Q^2)$ in QCD has indeed a power series expansion:

$$-\frac{t_0}{Q^2} \Pi(Q^2) \underset{Q^2 \rightarrow 0}{\sim} \mathcal{M}(0) - \frac{Q^2}{t_0} \mathcal{M}(-1) + \left(\frac{Q^2}{t_0}\right)^2 \mathcal{M}(-2) - \left(\frac{Q^2}{t_0}\right)^3 \mathcal{M}(-3) + \dots , \quad (3.4)$$

and the coefficients $\mathcal{M}(0), \mathcal{M}(-n), n = 1, 2, 3, \dots$ are precisely the moments of the spectral function defined in Eq. (2.3). Ramanujan's theorem implies then that

$$\int_0^\infty d\left(\frac{Q^2}{t_0}\right) \left(\frac{Q^2}{t_0}\right)^{s-1} \left\{ \mathcal{M}(0) - \frac{Q^2}{t_0} \mathcal{M}(-1) + \left(\frac{Q^2}{t_0}\right)^2 \mathcal{M}(-2) + \dots \right\} = \Gamma(s)\Gamma(1-s) \mathcal{M}(s), \quad (3.5)$$

and it allows, in principle, to reconstruct the Mellin transform $\mathcal{M}(s)$ in the full complex s -plane from just the knowledge of the discrete moments $\mathcal{M}(-n), n = 0, 1, 2, 3, \dots$.

Another interesting property of the Mellin transform in Eq. (2.7), based on the so called *Basic Abelian Theorem* [34], is the fact that the behaviour of the leading term in the expansion of $\mathcal{M}(-n)$ for $n \rightarrow \infty$, is correlated to the leading term in the threshold expansion of the spectral function $\frac{1}{\pi} \text{Im}\Pi(t)$ ⁵. In what follows we shall not implement this as a constraint but it can be used as a check of how well the successive parameterizations satisfy this threshold property.

⁵An application of this theorem to heavy quark correlators can be found in ref. [37].

III.1.1 A simple example: QED at the one loop level.

Let us illustrate Ramanujan's theorem with a simple example: the lowest order vacuum polarization in QED induced by a fermion of mass m . The Taylor expansion in this case is given by coefficients which are easily calculable:

$$-\frac{4m^2}{Q^2}\Pi^{\text{QED}}(Q^2) \underset{Q^2 \rightarrow 0}{\sim} \sum_{n=0,1,2,\dots} (-1)^n \left(\frac{Q^2}{4m^2}\right)^n \frac{\alpha}{\pi} \frac{1}{n+1} \frac{\sqrt{\pi}}{4} \frac{\Gamma(3+n)}{\Gamma(\frac{7}{2}+n)}, \quad (3.6)$$

and the moments of the lowest order QED spectral function are then

$$\mathcal{M}^{\text{QED}}(-n) = \frac{\alpha}{\pi} \frac{1}{n+1} \frac{\sqrt{\pi}}{4} \frac{\Gamma(3+n)}{\Gamma(\frac{7}{2}+n)}, \quad n = 0, 1, 2, 3, \dots \quad (3.7)$$

Ramanujan tells us that, without doing the analytical calculation of the full Mellin transform of the spectral function, one can get the result from the simple replacement $n \rightarrow -s$ in these moments and that gives the function $\mathcal{M}^{\text{QED}}(s)$ extended to the full s -plane i.e., the simple replacement:

$$\frac{\alpha}{\pi} \frac{1}{n+1} \frac{\sqrt{\pi}}{4} \frac{\Gamma(3+n)}{\Gamma(\frac{7}{2}+n)} \underset{(n \rightarrow -s)}{\Rightarrow} \frac{\alpha}{\pi} \frac{\sqrt{\pi}}{4} \frac{1}{1-s} \frac{\Gamma(3-s)}{\Gamma(\frac{7}{2}-s)} \equiv \mathcal{M}^{\text{QED}}(s), \quad (3.8)$$

gives the analytic result of the Mellin transform

$$\mathcal{M}^{\text{QED}}(s) = \int_{4m^2}^{\infty} \frac{dt}{t} \left(\frac{t}{4m^2}\right)^{s-1} \frac{1}{\pi} \text{Im}\Pi^{\text{QED}}(t), \quad (3.9)$$

where

$$\frac{1}{\pi} \text{Im}\Pi^{\text{QED}}(t) = \frac{\alpha}{\pi} \frac{1}{3} \left(1 + \frac{2m^2}{t}\right) \sqrt{1 - \frac{4m^2}{t}} \theta(t - 4m^2). \quad (3.10)$$

We shall soon come back to a discussion of further aspects of this simple QED example.

III.2 Marichev's Class of Mellin Transforms.

The class in question is the one defined by *standard products* of gamma functions of the type

$$\mathcal{M}(s) = C \prod_{i,j,k,l} \frac{\Gamma(a_i - s)\Gamma(c_j + s)}{\Gamma(b_k - s)\Gamma(d_l + s)}, \quad (3.11)$$

with constants C , a_i , b_k , c_j and d_l and where the Mellin variable s only appears with a \pm coefficient. The interesting thing about this class of functions is that all the Generalized Hypergeometric Functions have Mellin transforms of this type [35]. As a result, many functions have a representation in terms of Mellin-Barnes integrals involving linear combinations of standard products of the Marichev type in Eq. (3.11).⁶

The Mellin transform of the lowest order QED Spectral Function in Eq. (3.9) is certainly of this type, (notice that $\frac{1}{1-s} = \frac{\Gamma(1-s)}{\Gamma(2-s)}$)

$$\mathcal{M}^{\text{QED}}(s) = \frac{\alpha}{\pi} \frac{\sqrt{\pi}}{4} \frac{\Gamma(1-s)}{\Gamma(2-s)} \frac{\Gamma(3-s)}{\Gamma(\frac{7}{2}-s)}. \quad (3.12)$$

Furthermore, we observe that in this case, without explicitly knowing the QED Spectral Function $\frac{1}{\pi} \text{Im}\Pi^{\text{QED}}(t)$, it is possible to reconstruct its full Mellin transform $\mathcal{M}^{\text{QED}}(s)$ from the knowledge of just three moments which, for example, we can choose to be:

- The asymptotic behaviour of $\frac{1}{\pi} \text{Im}\Pi^{\text{QED}}(t)$ when $t \rightarrow \infty$ which requires that

$$\mathcal{M}^{\text{QED}}(s) \underset{s \rightarrow 1}{\sim} \frac{\alpha}{\pi} \frac{1}{3} \frac{1}{1-s}, \quad (3.13)$$

⁶For a helpful tutorial see e.g. ref. [36] and references therein.

- And the values of the first and second moments:

$$\mathcal{M}^{\text{QED}}(0) = \frac{\alpha}{\pi} \frac{4}{15} \quad \text{and} \quad \mathcal{M}^{\text{QED}}(-1) = \frac{\alpha}{\pi} \frac{4}{35}. \quad (3.14)$$

Indeed, setting $\mathcal{M}^{\text{QED}}(s)$ to be of the *particular* Marichev form:

$$\mathcal{M}^{\text{QED}}(s) \doteq \frac{\alpha}{\pi} \frac{1}{3} \frac{\Gamma(1-s)}{\Gamma(2-s)} \frac{\Gamma(c-1)}{\Gamma(c-s)} \frac{\Gamma(d-s)}{\Gamma(d-1)}, \quad (3.15)$$

which already incorporates the constraint in Eq. (3.13), and solving the matching conditions to the two moments in Eq. (3.14) results in two simple equations for the c and d parameters:

$$\frac{d-1}{c-1} = \frac{4}{5}, \quad \text{and} \quad \frac{d}{c} = \frac{6}{7} \quad (3.16)$$

with solutions $c = \frac{7}{2}$ and $d = 3$ and, therefore, the result in Eq. (3.12) follows. This is quite impressive. It means that the full shape of the Mellin transform $\mathcal{M}^{\text{QED}}(s)$ as a function of s , which is partly shown in Fig. (2), can be fully reconstructed from its knowledge at just three points, which in our case we have chosen to be the three dots in the figure corresponding to $s = 1$, $s = 0$ and $s = -1$.

In this particular QED example, the behaviour of the leading term in the expansion of $\mathcal{M}^{\text{QED}}(-n)$ for $n \rightarrow \infty$ is

$$\mathcal{M}^{\text{QED}}(-n) \underset{n \rightarrow \infty}{\sim} \frac{\alpha}{\pi} \frac{\sqrt{\pi}}{4} \frac{1}{n} n^{3-\frac{7}{2}} = \frac{\alpha}{\pi} \frac{\sqrt{\pi}}{4} n^\gamma, \quad \text{with} \quad \gamma = -3/2, \quad (3.17)$$

which, according to the Basic Abelian Theorem [34], and in terms of the threshold variable

$$\delta = \sqrt{1 - \frac{t_0}{t}}, \quad (3.18)$$

implies that

$$\text{Im}\Pi(t) \underset{\delta \rightarrow 0}{\sim} -\frac{\alpha}{\pi} \frac{\sqrt{\pi}}{4} \frac{1}{\delta^2} \Gamma(\gamma + 1) \delta^{-2\gamma}, \quad (3.19)$$

and reproduces the exact behaviour of the spectral function in Eq. (3.10) at threshold:

$$\frac{1}{\pi} \text{Im}\Pi^{\text{QED}}(t) \underset{t \rightarrow t_0}{\sim} \frac{\alpha}{\pi} \frac{1}{2} \delta. \quad (3.20)$$

III.3 Convergence Criteria of Mellin-Barnes Integrals.

It may not have escaped the attention of the alert reader that in the discussion of the previous QED example, the choice of Eq. (3.15) was a *particular* choice of a Marichev-like function. Why this choice and not one e.g. with all the Gamma functions in the numerator or in the denominator, and why not choices with $+s$ instead of $-s$? The reason for the *particular* choice we made is that, as already mentioned regarding the Mellin transform of the spectral function in QCD, the QED Mellin transform $\mathcal{M}^{\text{QED}}(s)$ is also a monotonously increasing function from $\text{Re}(s) = -\infty$ to $\text{Re}(s) = 1$. This implies that $\mathcal{M}^{\text{QED}}(s)$ cannot have either poles or zeros in the negative $\text{Re}(s)$ axis. Furthermore, the function $\Pi^{\text{QED}}(Q^2)$ is known to be analytic except for a cut from $t = 4m^2$ to $t = \infty$. These are very general properties, also shared by the QCD vacuum polarization function, which imply precise restrictions on the subclass of Marichev functions that one must use when trying to implement successive approximations and which we shall next discuss.

In that respect we have been particularly helped by some relatively recent mathematical literature [38, 39, 40]. The authors of these references have studied the general conditions for the convergence of a very general class of Mellin-Barnes integrals, which include those of the Marichev class, and their results can be summarized as follows.

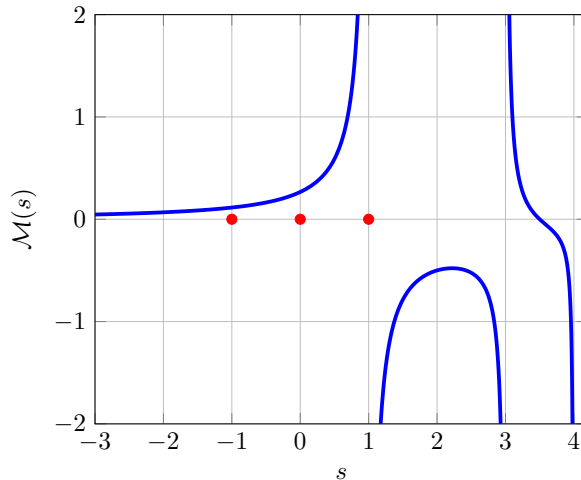


Figure 2:

Shape of the QED Mellin transform $\mathcal{M}^{\text{QED}}(s)$ (in blue) as a function of s . $\mathcal{M}^{\text{QED}}(s)$ is fully reconstructed from its knowledge at just the three red points.

Consider the rather general type of Mellin-Barnes integral

$$I(z) = \frac{1}{2\pi i} \int_{c-i\infty}^{c+i\infty} ds z^{-s} \frac{\prod_{j=1}^m \Gamma(A_j s + B_j)}{\prod_{k=1}^n \Gamma(C_k s + D_k)}. \quad (3.21)$$

In our case this will apply to the Mellin-Barnes integral in Eq. (2.11) where

$$z \equiv \frac{Q^2}{t_0} \quad \text{and} \quad I(z) \equiv -\frac{t_0}{Q^2} \Pi(Q^2), \quad (3.22)$$

as well as to the Mellin-Barnes integral in Eq. (2.15) where

$$z \equiv \frac{m_\mu^2}{t_0} \quad \text{and} \quad I(z) \equiv a_\mu^{\text{HVP}}(z). \quad (3.23)$$

Quite generally, the authors of refs. [38, 39] have studied the properties of the mapping which integrals like those in Eq. (3.21) establish between the Mellin s -plane and the z -plane. This is illustrated in Fig. (3) where the crosses denote the positions of the poles in the integrand of Eq. (3.21): in blue the poles at the left of the fundamental strip (represented by the green strip in the figure) and in red at the r.h.s. of the fundamental strip. In the z -plane we show the disc $|z| \leq R$ in blue, with R the radius of convergence, and the cut starting at $\text{Re}(z) \geq R$ ⁷. The converse mapping theorem of ref. [28] relates in a precise way the singularities in the complex s -plane of the integrand in Eq. (3.21) to the asymptotic expansions of $I(z)$ for z large (the red mapping in Fig. (3)) and for z small (the blue mapping in Fig. (3)). Following refs. [38, 39, 40] we are instructed to consider the two quantities:

$$\Delta \doteq \sum_{j=1}^m A_j - \sum_{k=1}^n C_k \quad \text{and} \quad \alpha \doteq \sum_{j=1}^m |A_j| - \sum_{k=1}^n |C_k|. \quad (3.24)$$

Then, the region where the integral $I(z)$ converges is $|\arg z| < \frac{\pi}{2} \alpha$ (see e.g. [38]), and there are three cases to be considered [39, 40]:

⁷For the sake of simplicity in drawing the figure, we assume that the disc of convergence is centered at $z = 0$ and that the cut starts at $\text{Re}(z) \geq R$.

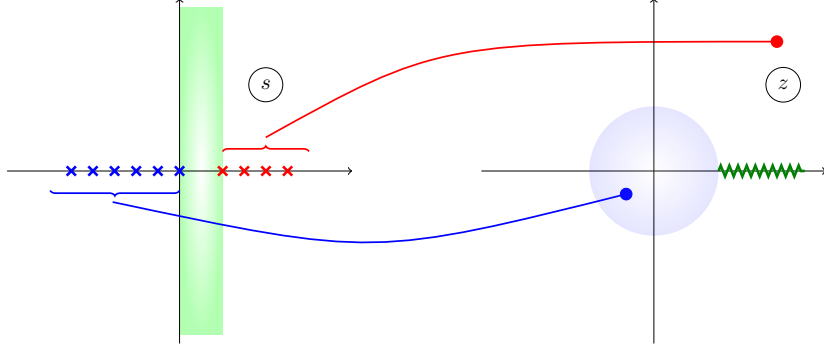


Figure 3:

Mapping of the Mellin s -Plane to the z -plane.

- If $\Delta > 0$, closing the integration contour to the left leads to a series representation of the integral $I(z)$ which converges for any value of z , but closing the contour to the right gives a divergent asymptotic expansion.
- If $\Delta < 0$, closing the contour to the right leads to a series representation of $I(z)$ which converges for any value of z , but closing the contour to the left gives a divergent asymptotic expansion.
- If $\Delta = 0$, closing the contour to the left and to the right gives two convergent series, the first series obtained by closing to the left converges within a disk $|z| < R$ whereas the other one converges outside this disk. Moreover, if $\alpha > 0$, the two series are the analytic continuation of each other.

These three cases are illustrated in Fig. (4).

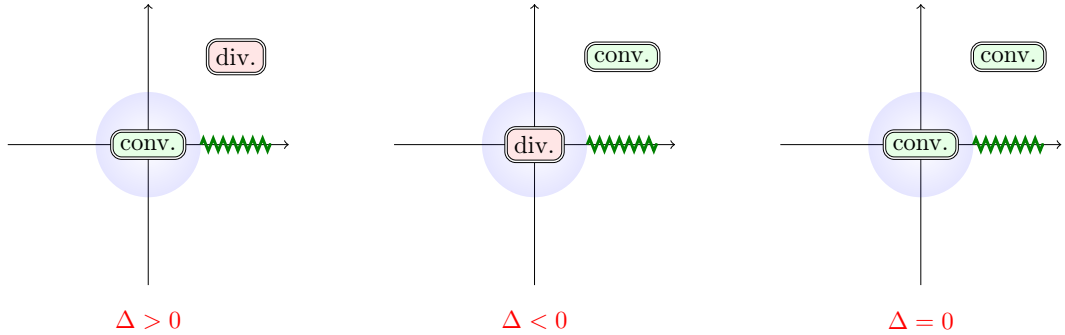


Figure 4:

*Behaviour of the series expansions of $I(z)$ depending on the sign of Δ for $|z| < R$ (the blue region) and $|z| > R$. The label *div.* denotes the regions where the asymptotic expansion is divergent or does not exist. The cut is represented by the green zigzag line.*

We are now in the position of fixing the class of successive Mellin approximants $\mathcal{M}_N(s)$ that we should use to ensure that they converge in the same way as the full QCD Mellin transform $\mathcal{M}(s)$ does. Associated to each $\mathcal{M}_N(s)$ approximant there will be a corresponding $\Pi_N(Q^2)$ approximant to $\Pi(Q^2)$ (via Eq. (2.11)) and, therefore, a corresponding $a_\mu^{\text{HVP}}(N)$ approximant to a_μ^{HVP} (via Eq. (2.20)). The input will be that we know the values of the first few moments

$$\mathcal{M}(0), \quad \mathcal{M}(-1), \quad \mathcal{M}(-2), \dots, \quad \mathcal{M}(-N+1), \quad (3.25)$$

including their errors and their correlation matrix, either from a LQCD determination or from a dedicated experiment. Given this input, we shall then restrict the successive Marichev-like Mellin approximants in Eq. (3.11) to those satisfying the following criteria:

1. The fundamental strip of each Mellin approximant $\mathcal{M}_N(s)$ must be the same as the one of the full Mellin transform $\mathcal{M}(s)$, so that the insertion of $\mathcal{M}_N(s)$ in the r.h.s. of Eq. (2.15) does not change the convergence region $c_s \equiv \text{Re}(s) \in]0, 1[$ of the exact Mellin transform.

In practice, due to the fact that the sequence of poles from $\Gamma(a_i - s)$ is at $s = a_i + n$ and the one from $\Gamma(c_j + s)$ at $s = -c_j - n$ with $n \in \mathbf{N}$ implies the restrictions:

$$\text{Re } a_i \geq 1 \quad \text{and} \quad \text{Re } c_j \geq 0. \quad (3.26)$$

2. The Mellin approximant $\mathcal{M}_N(s)$ should not generate poles nor zeros in the region $-\infty < \text{Re}(s) < 1$, where $\mathcal{M}(s)$ is known to be monotonously increasing. Since $\text{Re } c_j \geq 0$, no poles for $\text{Re}(s) < 1$ implies the absence of factors $\Gamma(c_j + s)$ or $j_{\max} = 0$. No zeros for $\mathcal{M}_N(s)$ in the region $-\infty < \text{Re}(s) < 1$ implies

$$\text{Re } b_k \geq 1. \quad (3.27)$$

3. We also want the corresponding $\Pi_N(Q^2)$ -function (see Eq. (3.33) below) to the Mellin approximant $\mathcal{M}_N(s)$ to converge for $z \equiv \frac{Q^2}{t_0}$ both for $|z| < 1$ and $|z| > 1$ which, according to the convergence conditions discussed above, requires that

$$\Delta = (1 - 1 - i_{\max}) - (-k_{\max} + l_{\max}) = k_{\max} - i_{\max} - l_{\max} = 0. \quad (3.28)$$

4. Finally, we want the two series generated by the $\Pi_N(Q^2)$ approximant for $|z| < 1$ and $|z| > 1$ to be the analytic continuation of each other which implies

$$\alpha = (2 + i_{\max}) - (k_{\max} + l_{\max}) > 0. \quad (3.29)$$

This, combined with Eq. (3.28), implies $l_{\max} < 1$ and hence the absence of $\Gamma(d_l + s)$ factors in the denominator of Eq. (3.11).

We therefore conclude that, in our case, the only Mellin approximants of the Marichev class that one must consider are those restricted to the subclass:

$$\mathcal{M}_N(s) = C_N \prod_{k=1}^N \frac{\Gamma(a_k - s)}{\Gamma(b_k - s)}, \quad (3.30)$$

with

$$\text{Re } a_k \geq 1 \quad \text{and} \quad \text{Re } b_k \geq 1. \quad (3.31)$$

From here onwards we shall simply call them Mellin-Barnes approximants (MBa).

Besides the matching to the input moments in Eq. (3.25), all the MBa that we shall use will be constrained to satisfy the leading pQCD short-distance behaviour ⁸

$$\mathcal{M}^{\text{QCD}}(s) \underset{s \rightarrow 1}{\sim} \frac{\alpha}{\pi} \left(\sum_i q_i^2 \right) \frac{1}{3} N_c \frac{1}{1-s}. \quad (3.32)$$

Given a MBa $\mathcal{M}_N(s)$, the corresponding $\Pi_N(Q^2)$ approximant to $\Pi(Q^2)$ is then

$$\Pi_N(Q^2) = -\frac{Q^2}{t_0} \frac{1}{2\pi i} \int_{c_s - i\infty}^{c_s + i\infty} ds \left(\frac{Q^2}{t_0} \right)^{-s} \Gamma(s)\Gamma(1-s) \mathcal{M}_N(s), \quad c_s \equiv \text{Re}(s) \in]0, 1[, \quad (3.33)$$

and the $a_\mu^{\text{HVP}}(N)$ approximant to a_μ^{HVP} will be given by the integral in Eq. (2.20) when inserting the corresponding $\mathcal{M}_N(\frac{1}{2} - i\tau)$ in the r.h.s. integrand. Notice that the factor $\mathcal{F}(s)$ does not modify the convergence criteria discussed above for $a_\mu^{\text{HVP}}(N)$, because $\mathcal{F}(s)$ has $\Delta = 0$ and $\alpha = 4$.

⁸It is possible to incorporate α_s corrections as well. They don't change, however, the residue of the pole at $s = 1$.

III.4 The $\Pi_N(Q^2)$ are Generalized Hypergeometric Functions, The $\text{Im}\Pi_N(t)$ are Meijer's G-Functions.

The Generalized Hypergeometric Function [41]

$${}_P F_Q[a_1, a_2, \dots, a_P; b_1, b_2, \dots, b_Q; z] \equiv {}_P F_Q \left(\begin{matrix} a_1 & a_2 & \dots & a_P \\ b_1 & b_2 & \dots & b_Q \end{matrix} \middle| z \right), \quad (3.34)$$

is defined, for $|z| < 1$, by the series

$$\begin{aligned} 1 + \frac{a_1 a_2 \dots a_P}{b_1 b_2 \dots b_Q} \frac{z}{1!} + \frac{a_1(a_1+1)a_2(a_2+1)\dots a_P(a_P+1)}{b_1(b_1+1)b_2(b_2+1)\dots b_Q(b_Q+1)} \frac{z^2}{2!} + \dots \\ \equiv \sum_{n=0}^{\infty} \frac{(a_1)_n (a_2)_n \dots (a_P)_n}{(b_1)_n (b_2)_n \dots (b_Q)_n} \frac{z^n}{n!}, \end{aligned} \quad (3.35)$$

where in the second line we use the Pochhammer symbol

$$(a)_n \equiv \frac{\Gamma(a+n)}{\Gamma(a)} = a(a+1)(a+2)\dots(a+n-1), \quad (3.36)$$

with in particular,

$$(a)_0 = 1, \quad \text{and} \quad (1)_n = n!. \quad (3.37)$$

This series has P numerator parameters, Q denominator parameters and one variable z . Any of these parameters are real or complex, but the b parameters must not be negative integers. The case where $P = 2$ and $Q = 1$ corresponds to the so called Gauss Hypergeometric Function. The sum of this type of series, when it exists, defines a Generalized Hypergeometric Function (GH-Function).

The reason why we are interested in GH-Functions is that, inserting the general expression in Eq. (3.30) for the $\mathcal{M}_N(s)$ approximant in the integrand of the r.h.s. in Eq. (3.33), and then doing the Mellin-Barnes integral over the s -variable, results in a specific GH-Function of the type:

$$\Pi_N(Q^2) = -\frac{Q^2}{t_0} C_N \prod_{k=1}^N \frac{\Gamma(a_k)}{\Gamma(b_k)} {}_{1+N} F_N \left(\begin{matrix} 1 & a_1 \dots & a_N \\ b_1 \dots & b_N \end{matrix} \middle| -\frac{Q^2}{t_0} \right), \quad (3.38)$$

which is given by the series in Eq. (3.35) for $|\frac{Q^2}{t_0}| < 1$, with its analytic continuation defined by the underlying Mellin-Barnes integral, Eq. (3.33) in this case. The corresponding Adler function is also a GH-Function:

$$\mathcal{A}_N(Q^2) \equiv -Q^2 \frac{\partial \Pi_N(Q^2)}{\partial(Q^2)} = \frac{Q^2}{t_0} C_N \prod_{k=1}^N \frac{\Gamma(a_k)}{\Gamma(b_k)} {}_{1+N} F_N \left(\begin{matrix} 2 & a_1 \dots & a_N \\ b_1 \dots & b_N \end{matrix} \middle| -\frac{Q^2}{t_0} \right). \quad (3.39)$$

The reason why we are interested in Meijer's G-Functions is that the inverse Mellin transform of $\mathcal{M}_N(s)$ corresponding to Eq. (2.7), i.e. the Mellin Barnes integrals

$$\frac{t_0}{t} \frac{1}{\pi} \text{Im} \Pi_N(t) = \frac{1}{2\pi i} \int_{c-i\infty}^{c+i\infty} ds \left(\frac{t}{t_0} \right)^{-s} \mathcal{M}_N(s), \quad c_s \equiv \text{Re}(s) \in]-\infty, 1[, \quad (3.40)$$

for arbitrary N and $t \geq t_0$ are a particular class of Meijer's G-Functions. Indeed, in full generality, Meijer's G-Functions are defined by a complex L -path integral (see e.g. *The Meijer G-Function* $G_{p,q}^{m,n} \left(z \middle| \begin{matrix} \mathbf{a} \\ \mathbf{b} \end{matrix} \right)$, in sect. 8.2 of ref. [42], pp. 617-626):

$$\begin{aligned} G_{p,q}^{m,n} \left(z \middle| \begin{matrix} 1-a_1, \dots, 1-a_n; a_{n+1}, \dots, a_p \\ b_1, \dots, b_m; 1-b_{m+1}, \dots, 1-b_q \end{matrix} \right) = \\ \frac{1}{2\pi i} \int_L ds z^{-s} \frac{\Gamma(b_1+s)\dots\Gamma(b_m+s)\cdot\Gamma(a_1-s)\dots\Gamma(a_n-s)}{\Gamma(a_{n+1}+s)\dots\Gamma(a_p+s)\cdot\Gamma(b_{m+1}-s)\dots\Gamma(b_q-s)}, \end{aligned} \quad (3.41)$$

and have the property that

$$\mathbf{G}_{p,q}^{0,n} \left(z \left| \begin{matrix} \mathbf{a} \\ \mathbf{b} \end{matrix} \right. \right) = 0 \text{ for } |z| < 1. \quad (3.42)$$

For the class of Marichev-like $\mathcal{M}_N(s)$ functions in Eq. (3.30) this results in a set of *equivalent* spectral functions:

$$\frac{1}{\pi} \text{Im}\Pi_N(t) = \frac{t}{t_0} C_N \mathbf{G}_{0,N}^{0,N} \left(\frac{t}{t_0} \left| \begin{matrix} 1 - a_1, \dots, 1 - a_N; \text{---} \\ \text{---}; 1 - b_1, \dots, 1 - b_N \end{matrix} \right. \right). \quad (3.43)$$

These successive *equivalent* spectral functions, alike the physical spectral function, are only defined for $t \geq t_0$ but they are not expected to reproduce point by point the detailed physical structure in the t -variable, until the level of approximation reaches the exact solution. They reproduce, however, the smooth behaviour of the self-energy functions $\Pi_N(Q^2)$ and of the Adler $\mathcal{A}_N(Q^2)$ functions when inserted in a dispersion relation and it is in this sense that we call them *equivalent*.

The explicit form of these general expressions for the first $N = 1$ and $N = 2$ cases are as follows:

- N=1

This corresponds to the case where we only know the first moment $\mathcal{M}(0)$. Then

$$\mathcal{M}_1(s) = C_1 \frac{\Gamma(a_1 - s)}{\Gamma(b_1 - s)}, \quad \text{with } C_1 = \frac{\alpha}{\pi} \frac{5}{3} \frac{N_c}{3} \Gamma(b_1 - 1) \quad \text{and } a_1 = 1 \quad (3.44)$$

to ensure the pQCD pole behaviour at $s = 1$. With b_1 fixed by the matching condition $\mathcal{M}_1(0) = \mathcal{M}(0)$ one finds

$$\Pi_1(Q^2) = -\frac{Q^2}{t_0} C_1 \frac{1}{\Gamma(b_1)} {}_2F_1 \left(\begin{matrix} 1 & a_1 \\ & b_1 \end{matrix} \left| -\frac{Q^2}{t_0} \right. \right), \quad (3.45)$$

and the corresponding Adler function [see Eq. (2.12)] is

$$\mathcal{A}_1(Q^2) = -Q^2 \frac{\partial \Pi_1(Q^2)}{\partial(Q^2)} = \frac{Q^2}{t_0} C_1 \frac{1}{\Gamma(b_1)} {}_2F_1 \left(\begin{matrix} 2 & a_1 \\ & b_1 \end{matrix} \left| -\frac{Q^2}{t_0} \right. \right), \quad (3.46)$$

with an *equivalent* spectral function:

$$\frac{1}{\pi} \text{Im}\Pi_1(t) = \frac{t}{t_0} C_1 \mathbf{G}_{0,1}^{0,1} \left(\frac{t}{t_0} \left| \begin{matrix} 1 - a_1; \text{---} \\ \text{---}; 1 - b_1 \end{matrix} \right. \right). \quad (3.47)$$

- N=2

This corresponds to the case where we know the first two moments $\mathcal{M}(0)$ and $\mathcal{M}(-1)$. Then

$$\mathcal{M}_2(s) = C_2 \frac{\Gamma(1-s) \Gamma(a_2 - s)}{\Gamma(2-s) \Gamma(b_2 - s)} \quad \text{with } C_2 = \frac{\alpha}{\pi} \frac{5}{3} \frac{N_c}{3} \frac{\Gamma(b_2 - 1)}{\Gamma(a_2 - 1)}, \quad (3.48)$$

and the parameters a_2 and b_2 fixed by the two matching conditions

$$\mathcal{M}_2(0) = \mathcal{M}(0) \quad \text{and} \quad \mathcal{M}_2(-1) = \mathcal{M}(-1). \quad (3.49)$$

Then

$$\Pi_2(Q^2) = -\frac{Q^2}{t_0} C_2 \frac{\Gamma(a_2)}{\Gamma(b_2)} {}_3F_2 \left(\begin{matrix} 1 & 1 & a_2 \\ & 2 & b_2 \end{matrix} \left| -\frac{Q^2}{t_0} \right. \right); \quad (3.50)$$

the corresponding Adler function is

$$\mathcal{A}_2(Q^2) = -Q^2 \frac{\partial \Pi_2(Q^2)}{\partial(Q^2)} = \frac{Q^2}{t_0} C_2 \frac{\Gamma(a_2)}{\Gamma(b_2)} {}_3F_2 \left(\begin{matrix} 2 & 1 & a_2 \\ & 2 & b_2 \end{matrix} \left| -\frac{Q^2}{t_0} \right. \right), \quad (3.51)$$

and the *equivalent* $N = 2$ spectral function is ⁹:

$$\frac{1}{\pi} \text{Im}\Pi_2(t) = \frac{t}{t_0} C_2 \mathbf{G}_{0,2}^{0,2} \left(\frac{t}{t_0} \left| \begin{matrix} 0, 1 - a_2; \text{---} \\ \text{---}; -1, 1 - b_2 \end{matrix} \right. \right). \quad (3.52)$$

⁹By contrast, the *equivalent* spectral function of the Padé approximant constructed with $\mathcal{M}(0)$ and $\mathcal{M}(-1)$ is just a delta function.

In the particular case of the lowest order vacuum polarization in QED discussed above, we have ($c_s \equiv \text{Re}(s) \in]0, 1[$):

$$\Pi^{\text{QED}}(Q^2) = -\frac{\alpha}{\pi} \frac{1}{3} \Gamma(5/2) \frac{Q^2}{4m^2} \frac{1}{2\pi i} \int_{c_s - i\infty}^{c_s + i\infty} ds \left(\frac{Q^2}{4m^2} \right)^{-s} \Gamma(s) \Gamma(1-s) \frac{\Gamma(1-s) \Gamma(3-s)}{\Gamma(2-s) \Gamma(\frac{7}{2}-s)}, \quad (3.53)$$

which is a typical $N = 2$ case, with $a_2 = 3$ and $b_2 = \frac{7}{2}$. Then, setting $z \equiv \frac{Q^2}{4m^2}$, one finds

$$\Pi^{\text{QED}}(Q^2) = -\frac{\alpha}{\pi} \frac{1}{3} \Gamma\left(\frac{5}{2}\right) \frac{\Gamma(3)}{\Gamma(7/2)} z {}_3F_2\left(\begin{matrix} 1 & 1 & 3 \\ & 2 & 7/2 \end{matrix} \middle| -z\right) \quad (3.54)$$

$$= \frac{\alpha}{\pi} \frac{(-3 + 5z) \sqrt{z} + 3(1 - 2z) \sqrt{1+z} \text{ArcSinh}(\sqrt{z})}{9z^{3/2}}. \quad (3.55)$$

In this case the GH-function has an explicit analytic form, which we give in the second line, and it coincides with the well known QED result. Notice that for $z = -\frac{t}{4m^2}$ with $t \geq 4m^2$, this expression develops an imaginary part which coincides with the Meijer's G-Function representation

$$\frac{1}{\pi} \text{Im} \Pi^{\text{QED}}(t) = \frac{t}{t_0} \frac{\alpha}{\pi} \frac{1}{3} \Gamma\left(\frac{5}{2}\right) G_{0,2}^{0,2}\left(\begin{matrix} t \\ t_0 \end{matrix} \middle| \begin{matrix} 0, -2; - \\ -; -1, -\frac{5}{2} \end{matrix}\right), \quad (3.56)$$

and reproduces the exact spectral function in Eq. (3.10).

Obviously, QED at lowest order is a very particular example where it just happens that one can reconstruct the exact function already at the level of the $N = 2$ MBa. In the next section we discuss a much more complicated example.

iv Mellin-Barnes-approximants (MBa) in QED at two loops.

We wish to test the techniques developed in the previous section with a more complicated example than the lowest order QED vacuum polarization. We suggest to examine the case of the QED vacuum polarization at two loops. The proper fourth order QED spectral function was first calculated by Källen and Sabry in 1955 [43] and later on in ref. [44]. It is given by the following expression:

With

$$\delta = \sqrt{1 - \frac{4m^2}{t}}, \quad (4.1)$$

$$\begin{aligned} \frac{1}{\pi} \text{Im} \Pi_{4\text{th}}^{\text{QED}}(t) &= \left(\frac{\alpha}{\pi}\right)^2 \left\{ \delta \left(\frac{5}{8} - \frac{3}{8} \delta^2 - \left(\frac{1}{2} - \frac{1}{6} \delta^2 \right) \log \left[64 \frac{\delta^4}{(1-\delta^2)^3} \right] \right) \right. \\ &+ \left(\frac{11}{16} + \frac{11}{24} \delta^2 - \frac{7}{48} \delta^4 + \left(\frac{1}{2} + \frac{1}{3} \delta^2 - \frac{1}{6} \delta^4 \right) \log \left[\frac{(1+\delta)^3}{8\delta^2} \right] \right) \log \left[\frac{1+\delta}{1-\delta} \right] \\ &+ 2 \left(\frac{1}{2} + \frac{1}{3} \delta^2 - \frac{1}{6} \delta^4 \right) \left(2 \text{Li}_2 \left[\frac{1-\delta}{1+\delta} \right] + \text{Li}_2 \left[-\frac{1-\delta}{1+\delta} \right] \right) \left. \right\} \theta(t - 4m^2). \quad (4.2) \end{aligned}$$

The asymptotic behaviours of this spectral function are

$$\frac{1}{\pi} \text{Im} \Pi_{4\text{th}}^{\text{QED}}(t) \underset{t \rightarrow 4m^2}{\sim} \left(\frac{\alpha}{\pi}\right)^2 \left\{ \frac{\pi^2}{4} - 2\sqrt{\frac{t}{4m^2} - 1} + \frac{\pi^2}{6} \left(\frac{t}{4m^2} - 1 \right) + \mathcal{O} \left[\left(\frac{t}{4m^2} - 1 \right)^{3/2} \right] \right\}, \quad (4.3)$$

$$\frac{1}{\pi} \text{Im} \Pi_{4\text{th}}^{\text{QED}}(t) \underset{t \rightarrow \infty}{\sim} \left(\frac{\alpha}{\pi}\right)^2 \left\{ \frac{1}{4} + \frac{3}{4} \frac{4m^2}{t} + \mathcal{O} \left[\left(\frac{4m^2}{t} \right)^2 \log \left(\frac{t}{4m^2} \right) \right] \right\}. \quad (4.4)$$

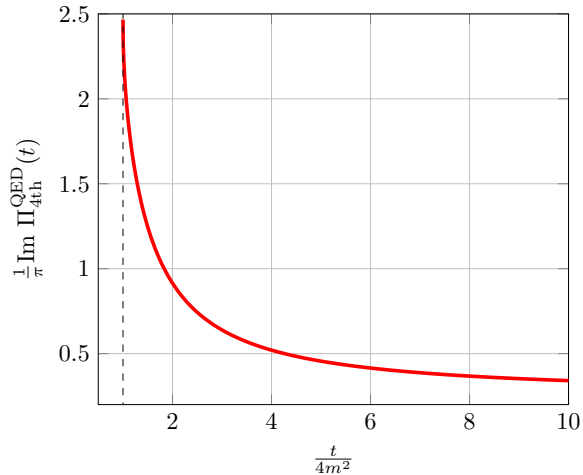


Figure 5:

Shape of the Spectral Function in Eq. (4.2) in $(\frac{\alpha}{\pi})^2$ units.

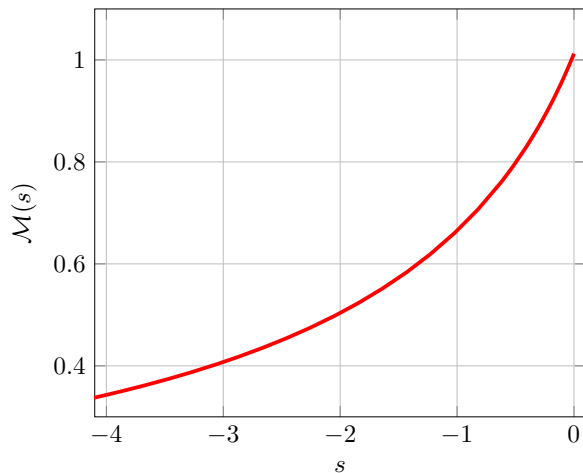


Figure 6:

Shape of the Mellin Transform of the Spectral Function in Eq. (4.2) in $(\frac{\alpha}{\pi})^2$ units.

Notice that the behaviour at threshold $t \sim 4m^2$ is rather different to the lowest order one and the shape of the spectral function, which is shown in Fig. (5), is also very different.

The shape of the Mellin transform of the 4th order spectral function in Eq. (4.2) is shown in Fig. (6). Like the Mellin transform of QCD it is also singular at $s = 1$ but with a different residue

$$\mathcal{M}_{4\text{th}}^{\text{QED}}(s) \underset{s \rightarrow 1}{\sim} \left(\frac{\alpha}{\pi}\right)^2 \frac{1}{4} \frac{1}{1-s}, \quad (4.5)$$

and shares with QCD the property of being a monotonously increasing function from $s = -\infty$ to $s < 1$.

The real part of the fourth order vacuum polarization in QED is also known analytically [43]. It is a rather complicated expression and, therefore, it is a good test to see how well it is approximated

by the successive GH-Functions in Eq. (3.38). The shape of the $\Pi_{4\text{th}}^{\text{QED}}(Q^2)$ function in the Euclidean is shown in Fig. (7).

We shall discuss this 4th order QED example in a way as close as possible to the QCD case which we shall later be confronted with. Therefore, the input will be the successive values of the moments of the spectral function, i.e. of the derivatives of $\Pi_{4\text{th}}^{\text{QED}}(Q^2)$ at $Q^2 = 0$.

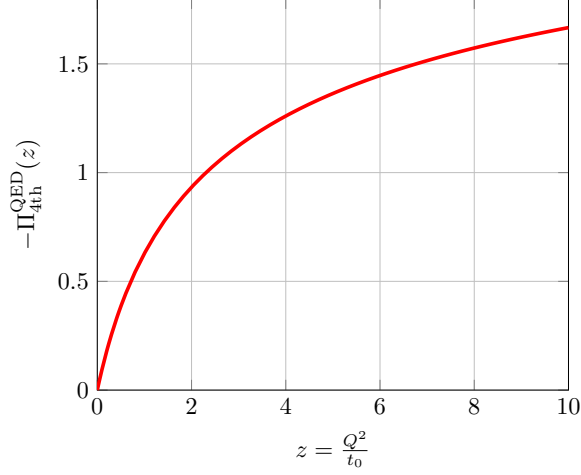


Figure 7:

Shape of the 4th order QED vacuum polarization function in the Euclidean $(\frac{\alpha}{\pi})^2$ units.

The first few Mellin moments

$$\mathcal{M}_{4\text{th}}^{\text{QED}}(s) \equiv \int_{t_0}^{\infty} \frac{dt}{t} \left(\frac{t}{t_0} \right)^{s-1} \frac{1}{\pi} \text{Im} \Pi_{4\text{th}}^{\text{QED}}(t), \quad (4.6)$$

for $s = 0, -1, -2, -3, -4, -5$, in units of $(\frac{\alpha}{\pi})^2$ are tabulated below in Table (1).

Table 1: $\mathcal{M}(s)$ Moments in units of $(\frac{\alpha}{\pi})^2$.

Moment	Exact result	Numerical value
$\mathcal{M}(0)$	81/82	1.012356796
$\mathcal{M}(-1)$	449/675	0.665185185
$\mathcal{M}(-2)$	249916/496125	0.503735936
$\mathcal{M}(-3)$	51986/127575	0.407493631
$\mathcal{M}(-4)$	432385216/1260653625	0.342984946
$\mathcal{M}(-5)$	5415247216/18261468225	0.296539531

IV.1 Successive Approximations to $\mathcal{M}_{4\text{th}}^{\text{QED}}(s)$, $\Pi_{4\text{th}}^{\text{QED}}(Q^2)$ and a_{μ}^{VP} .

We can now proceed to the construction of a successive set of MBa's to $\mathcal{M}_{4\text{th}}^{\text{QED}}(s)$ of the type shown in Eq. (3.30) and to the evaluation of the corresponding GH-function approximation to $\Pi_{4\text{th}}^{\text{QED}}(Q^2)$ of the type shown in Eq. (3.38). At each approximation step we shall then evaluate the corresponding contribution to the anomalous magnetic moment of a fermion of mass m induced by the 4th order

vacuum polarization generated by the same fermion (see the corresponding Feynman diagrams in Fig. (8)), and compare it with the exact result which is known analytically [45]:

$$a_\mu^{\text{VP}} = \left(\frac{\alpha}{\pi}\right)^3 \left\{ \frac{673}{108} - \frac{41}{81}\pi^2 - \frac{4}{9}\pi^2 \log(2) - \frac{4}{9}\pi^2 \log^2(2) + \frac{4}{9}\log^4(2) - \frac{7}{270}\pi^4 + \frac{13}{18}\zeta(3) + \frac{32}{3}\text{PolyLog}\left[4, \frac{1}{2}\right] \right\} = \left(\frac{\alpha}{\pi}\right)^3 0.0528707. \quad (4.7)$$

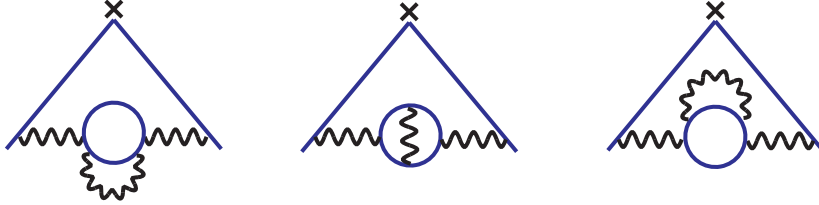


Figure 8:
Feynman diagrams contributing to the muon anomaly in Eq. (4.7).

The result in Eq. (4.7) is a rather complicated expression involving higher transcendental numbers with important numerical cancellations among the different terms and, therefore, it should provide a good test. We want to investigate how well we reproduce this exact result using the Mellin-Barnes integral representation in Eq. (2.20) which, when adapted to this case, reads as follows:

$$a^{\text{VP}(N)} = \left(\frac{\alpha}{\pi}\right) \frac{1}{2} \frac{1}{2\pi} \int_{-\infty}^{+\infty} d\tau e^{i\tau \log \frac{1}{4}} \mathcal{F}\left(\frac{1}{2} - i\tau\right) \mathcal{M}_N\left(\frac{1}{2} - i\tau\right), \quad (4.8)$$

with $\mathcal{M}_N(s)$ the successive Mellin approximants.

IV.1.1 The $N = 1$ MBa.

This corresponds to the case where we only know $\mathcal{M}_{4\text{th}}^{\text{QED}}(0)$. Following Eq. (3.30) we are instructed to consider as a first Mellin approximant:

$$\mathcal{M}_{4\text{th}}^{\text{QED}}(s) \Rightarrow \mathcal{M}_1(s) = C_1 \frac{\Gamma(a-s)}{\Gamma(b-s)}, \quad (4.9)$$

which must be singular at $s = 1$. This fixes the a parameter to $a = 1$ and the overall normalization to

$$C_1 = \left(\frac{\alpha}{\pi}\right)^2 \frac{1}{4} \Gamma(b-1), \quad (4.10)$$

so as to reproduce the leading singularity when $s \rightarrow 1$. Matching $\mathcal{M}_1(s)$ at $s = 0$ with the numerical value of $\mathcal{M}_{4\text{th}}^{\text{QED}}(0)$ in Table (1) fixes the b parameter to

$$b = 1.24695122. \quad (4.11)$$

We can then perform the corresponding integral in Eq. (4.8) which gives as a result for the first $N = 1$ approximant:

$$a^{\text{VP}(N=1)} = \left(\frac{\alpha}{\pi}\right)^3 \times 0.0500007. \quad (4.12)$$

It already reproduces the Mignaco-Remiddi exact result in Eq. (4.7) to an accuracy of 5%.

IV.1.2 The $N = 2$ MBa.

This corresponds to the case where we know the slope and curvature of $\Pi_{4\text{th}}^{\text{QED}}(Q^2)$ at $Q^2 = 0$, i.e. $\mathcal{M}_{4\text{th}}^{\text{QED}}(0)$ and $\mathcal{M}_{4\text{th}}^{\text{QED}}(-1)$. This information is similar to that already available from LQCD¹⁰. We shall therefore discuss it in detail.

The Mellin approximant in this case has two parameters a and b :

$$\mathcal{M}_{4\text{th}}^{\text{QED}}(s) \Rightarrow \mathcal{M}_2(s) = C_2 \frac{\Gamma(1-s) \Gamma(a-s)}{\Gamma(2-s) \Gamma(b-s)}, \quad (4.13)$$

and the leading short-distance constraint fixes the overall normalization to

$$C_2 = \left(\frac{\alpha}{\pi}\right)^2 \frac{1}{4} \frac{\Gamma(b-1)}{\Gamma(a-1)}, \quad (4.14)$$

with the parameters a and b fixed by the two matching equations:

$$\frac{1}{4} \frac{a-1}{b-1} = \mathcal{M}_{4\text{th}}^{\text{QED}}(0) \quad \text{and} \quad \frac{1}{8} \frac{a}{b} \frac{a-1}{b-1} = \mathcal{M}_{4\text{th}}^{\text{QED}}(-1), \quad (4.15)$$

or equivalently

$$\frac{1}{4} \frac{a-1}{b-1} = \mathcal{M}_{4\text{th}}^{\text{QED}}(0) \quad (4.16)$$

$$\frac{1}{2} \frac{a}{b} = \frac{\mathcal{M}_{4\text{th}}^{\text{QED}}(-1)}{\mathcal{M}_{4\text{th}}^{\text{QED}}(0)}. \quad (4.17)$$

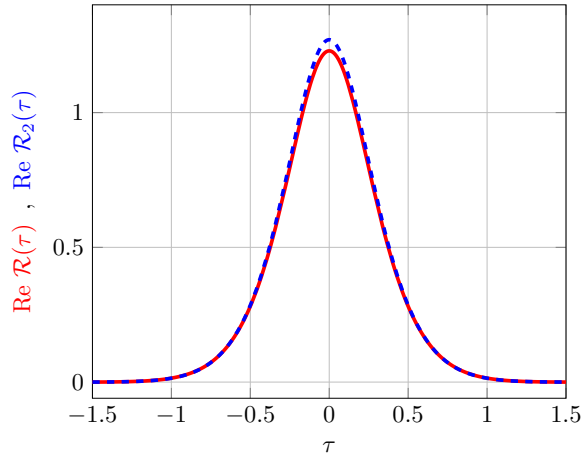


Figure 9:

*Plot of the real part of the integrand $\mathcal{R}_2(\tau)$ in Eq. (4.19):
the red curve corresponds to inserting the exact $\mathcal{M}_{4\text{th}}^{\text{QED}}(\frac{1}{2} - i\tau)$ in the integrand
the dashed blue curve from inserting the approximation $\mathcal{M}_2(\frac{1}{2} - i\tau)$.*

Inserting the numerical values in Table (1) for $\mathcal{M}_{4\text{th}}^{\text{QED}}(0)$ and $\mathcal{M}_{4\text{th}}^{\text{QED}}(-1)$ results in the values

$$a = 1.46508 \quad \text{and} \quad b = 1.11485. \quad (4.18)$$

¹⁰See refs. [11, 12, 13] and references therein.

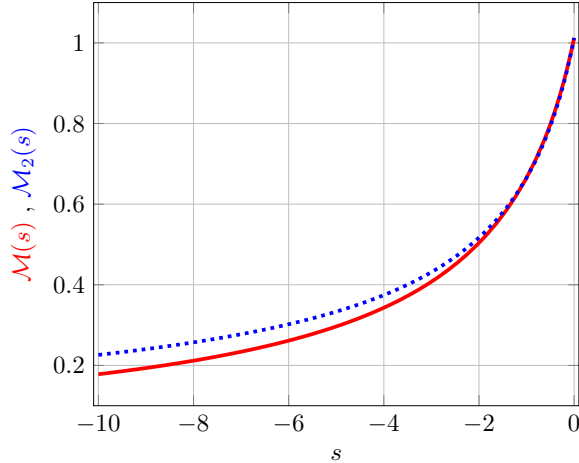


Figure 10:

The red curve is the Mellin Transform of the Spectral Function in Eq. (4.2).

The dotted blue curve is the $N = 2$ Mellin approximant in Eq. (4.13).

Both curves are shown in $(\frac{\alpha}{\pi})^2$ units.

With these parameter values inserted in $\mathcal{M}_2(s)$ in Eq. (4.13), and performing the corresponding integral in Eq. (4.8), i.e. the integral

$$a_{\mu}^{\text{VP}}(N=2) = \left(\frac{\alpha}{\pi}\right) \frac{1}{2} \frac{1}{2\pi} \int_{-\infty}^{+\infty} d\tau \underbrace{e^{i\tau \log(4)} \mathcal{F}\left(\frac{1}{2} - i\tau\right) \mathcal{M}_2\left(\frac{1}{2} - i\tau\right)}_{\mathcal{R}_2(\tau)}, \quad (4.19)$$

gives the result

$$a^{\text{VP}}(N=2) = \left(\frac{\alpha}{\pi}\right)^3 \times 0.0531447, \quad (4.20)$$

which reproduces the Mignaco-Remiddi result in Eq. (4.7) to an accuracy of 0.5%, a significant improvement with respect to the $N = 1$ approximant. Figure (9) shows the behaviour of the real part of the integrand $\mathcal{R}_2(\tau)$ in Eq. (4.19) as a function of τ , where the red curve is the one when one inserts the exact Mellin transform $\mathcal{M}_{4\text{th}}^{\text{QED}}(\frac{1}{2} - i\tau)$ in the integrand and the dashed blue curve the one associated to the $N = 2$ approximation. Already at this level of approximation the agreement between both integrands is quite impressive.

At this stage it is also interesting to compare the exact Mellin transform shown in Fig (6) with the one corresponding to the $N = 2$ approximation. This is shown in Fig. (10) where the blue dotted curve is the $N = 2$ approximation. The agreement of the two curves down to $s \simeq -3$ is quite remarkable. In order to see the difference between these two curves we show in Fig. (11) the plot of their ratio. The $\mathcal{M}_2(s)/\mathcal{M}(s)$ ratio turns out to be greater than one everywhere, except in the interval $-1 \leq s \leq 0$. This is why the $N = 2$ result approaches the exact value of the anomaly from above. The quality of the interpolation between $s = 0$ and $s = -1$ provided by the $N = 2$ approximation is shown at the right in Fig. (11). Notice the scale in the figure, e.g. the value at the minimum of the ratio shown in this figure is 0.9937 compared to one.

According to Eq. (3.38), the $N = 2$ GH-function approximant to $\Pi_{4\text{th}}^{\text{QED}}(Q^2)$ is given by the expression ($z \equiv \frac{Q^2}{i_0}$):

$$\Pi_{4\text{th}}^{\text{QED}}(Q^2) \Rightarrow \Pi_{(N=2)}^{\text{QED}}(Q^2) = \left(\frac{\alpha}{\pi}\right)^2 (-z) \frac{1}{4} \frac{a-1}{b-1} {}_3F_2 \left(\begin{matrix} 1 & 1 & a \\ & 2 & b \end{matrix} \middle| -z \right), \quad (4.21)$$

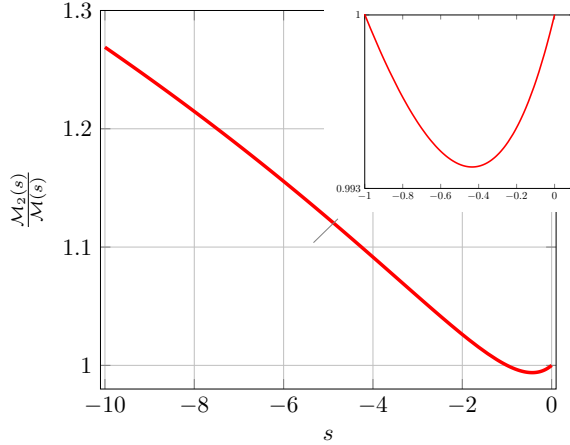


Figure 11:

Plots of the ratio $\frac{\mathcal{M}_2(s)}{\mathcal{M}(s)}$ versus s . Notice the scale of the plots.

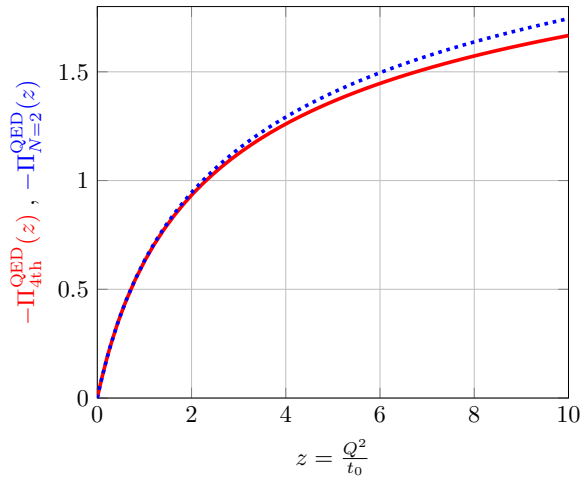


Figure 12:

The red curve is the exact 4th order QED VP-function.

The dotted blue curve is the $N = 2$ approximant.

Both curves are shown in $(\frac{\alpha}{\pi})^2$ units.

where ${}_3F_2\left(\begin{matrix} 1 & 1 & a \\ 2 & b \end{matrix} \middle| -z\right)$ is the GH-Function defined by the series:

$${}_3F_2\left(\begin{matrix} 1 & 1 & a \\ 2 & b \end{matrix} \middle| -z\right) = \sum_{n=0}^{\infty} \frac{(1)_n(1)_n(a)_n}{(2)_n(b)_n} \frac{(-z)^n}{n!}, \quad (4.22)$$

and a and b have the values given in Eq. (2.20). Figure (12) shows how well the MBa $\Pi_{(N=2)}^{\text{QED}}(Q^2)$ (blue curve) does when compared to the exact function (red curve). From this comparison, one can qualitatively understand why the $N = 2$ approximation already reproduces the exact value of a^{VP} in Eq. (4.7) at the 0.5% level.

The *equivalent* spectral function corresponding to the $N = 2$ approximation is given by the Meijer's

G-Function:

$$\frac{1}{\pi} \text{Im} \Pi_2(t) = \frac{t}{t_0} \left(\frac{\alpha}{\pi} \right)^2 \frac{1}{4} G_{0,2}^{0,2} \left(\frac{t}{t_0} \middle| \begin{matrix} 0, 1-a; \\ -1, 1-b \end{matrix} \right), \quad (4.23)$$

and its shape, compared to the exact spectral function, is shown in Fig. (13).

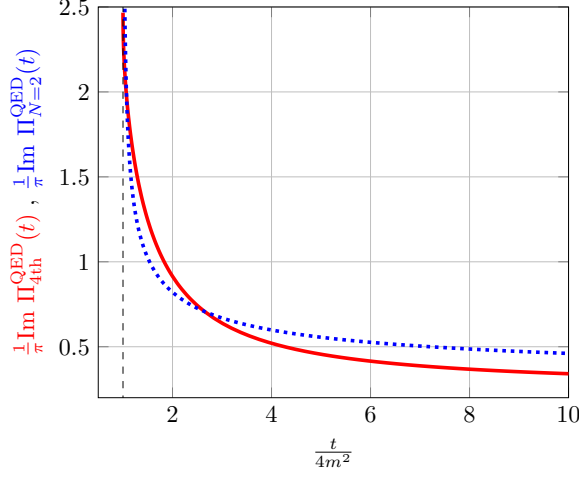


Figure 13:

*The red curve is the exact 4th order QED spectral function.
The dotted blue curve is the $N = 2$ approximant.
Both curves are shown in $\left(\frac{\alpha}{\pi}\right)^2$ units.*

IV.1.3 The $N = 3$ MBa.

This corresponds to the Mellin approximant

$$\mathcal{M}_{4\text{th}}^{\text{QED}}(s) \Rightarrow \mathcal{M}_3(s) = C_3 \frac{\Gamma(1-s)\Gamma(a_1-s)}{\Gamma(b_1-s)\Gamma(b_2-s)}, \quad (4.24)$$

with

$$C_3 = \left(\frac{\alpha}{\pi} \right)^2 \frac{1}{4} \frac{\Gamma(b_1-1)\Gamma(b_2-1)}{\Gamma(a_1-1)}, \quad (4.25)$$

and the three parameters a_1 , a_2 and b_1 fixed by matching $\mathcal{M}_3(s)$ to the values of the three moments $\mathcal{M}_{4\text{th}}^{\text{QED}}(0)$, $\mathcal{M}_{4\text{th}}^{\text{QED}}(-1)$, and $\mathcal{M}_{4\text{th}}^{\text{QED}}(-2)$. The matching equations in this case are:

$$\left(\frac{\alpha}{\pi} \right)^2 \frac{1}{4} \frac{1}{b_1-1} (a_1-1) \frac{1}{b_2-1} = \mathcal{M}_{4\text{th}}^{\text{QED}}(0), \quad (4.26)$$

$$\frac{1}{b_1} a_1 \frac{1}{b_2} = \frac{\mathcal{M}_{4\text{th}}^{\text{QED}}(-1)}{\mathcal{M}_{4\text{th}}^{\text{QED}}(0)}, \quad (4.27)$$

$$2 \frac{1}{b_1+1} (a_1+1) \frac{1}{b_2+1} = \frac{\mathcal{M}_{4\text{th}}^{\text{QED}}(-2)}{\mathcal{M}_{4\text{th}}^{\text{QED}}(-1)}, \quad (4.28)$$

which results in the values:

$$a_1 = 2.528554853, \quad b_1 = 1.163614902, \quad b_2 = 3.307115556, \quad (4.29)$$

or the equivalent solution with $b_1 \rightleftharpoons b_2$. With these values inserted in $\mathcal{M}_3(s)$ in Eq. (4.13), and performing the corresponding integral in Eq. (4.8) gives the result

$$a^{\text{VP}}(N=3) = \left(\frac{\alpha}{\pi}\right)^3 \times 0.0528678, \quad (4.30)$$

which now reproduces the Mignaco-Remiddi result in Eq. (4.7) to the remarkable accuracy of 0.004%.

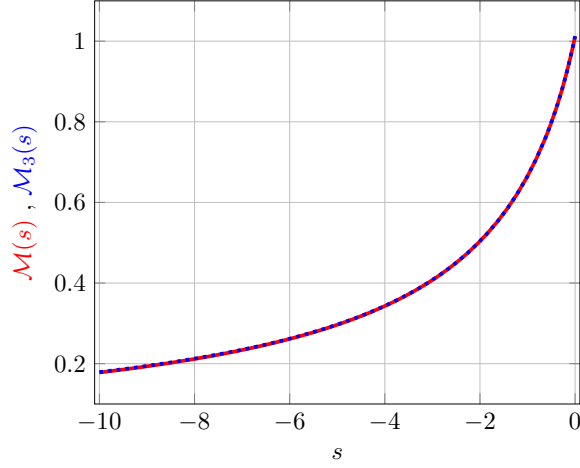


Figure 14:

The red curve is the Mellin Transform of the exact Spectral Function. The dashed blue curve is the $N=3$ Mellin approximant. Both curves are shown in $\left(\frac{\alpha}{\pi}\right)^2$ units.

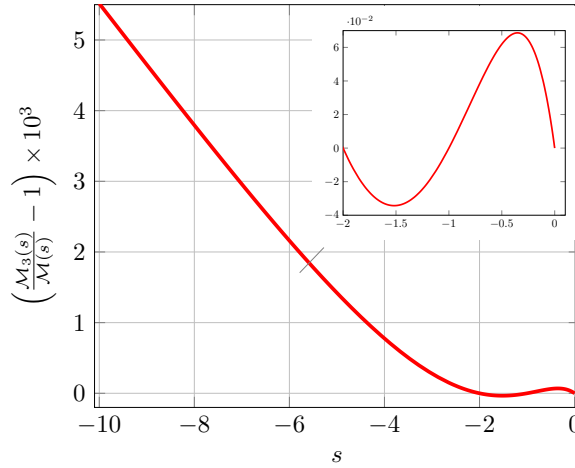


Figure 15:

Plots of the ratio $\frac{\mathcal{M}_3(s)}{\mathcal{M}(s)}$ versus s . Notice the vertical scales of these plots.

As an illustration of the quality of the approximation, we show in Fig. (14) the Mellin transform of the $N=3$ approximation (the blue dashed curve) compared to the exact Mellin transform (the red curve). At the scale of the figure it is practically impossible to see the difference. In order to see that, we show plots of the ratio $\mathcal{M}_3(s)/\mathcal{M}(s)$ in Fig. (15). Notice the scale in the left plot of Fig. (15)

as compared to the one in Fig. (11) and the improvement in the figure at the right which is plotted at the same scale as Fig. (11).

An accuracy of 0.004% is already much beyond what is required of the HVP contribution to the muon anomaly in QCD, but for the sake of testing the approximation procedure that we are advocating, let us try further possible improvements.

IV.1.4 The $N = 4$ MBa.

The $N = 4$ approximant is

$$\mathcal{M}_{4\text{th}}^{\text{QED}}(s) \Rightarrow \mathcal{M}_4(s) = C_4 \frac{\Gamma(1-s)\Gamma(a_1-s)\Gamma(a_2-s)}{\Gamma(2-s)\Gamma(b_1-s)\Gamma(b_2-s)}, \quad (4.31)$$

with

$$C_4 = \left(\frac{\alpha}{\pi}\right)^2 \frac{1}{4} \frac{\Gamma(b_1-1)\Gamma(b_2-1)}{\Gamma(a_1-1)\Gamma(a_2-1)}, \quad (4.32)$$

and the four parameters a_1 , a_2 , b_1 and b_2 solutions of the matching equations:

$$\frac{1}{4} \frac{a_1-1}{b_1-1} \frac{a_2-1}{b_2-1} = \mathcal{M}_{4\text{th}}^{\text{QED}}(0), \quad (4.33)$$

$$\frac{1}{2} \frac{a_1}{b_1} \frac{a_2}{b_2} = \frac{\mathcal{M}_{4\text{th}}^{\text{QED}}(-1)}{\mathcal{M}_{4\text{th}}^{\text{QED}}(0)}, \quad (4.34)$$

$$\frac{2}{3} \frac{(a_1+1)}{(b_1+1)} \frac{(a_2+1)}{(b_2+1)} = \frac{\mathcal{M}_{4\text{th}}^{\text{QED}}(-2)}{\mathcal{M}_{4\text{th}}^{\text{QED}}(-1)}, \quad (4.35)$$

$$\frac{3}{4} \frac{(a_1+2)}{(b_1+2)} \frac{(a_2+2)}{(b_2+2)} = \frac{\mathcal{M}_{4\text{th}}^{\text{QED}}(-3)}{\mathcal{M}_{4\text{th}}^{\text{QED}}(-2)}, \quad (4.36)$$

which give the values:

$$a_1 = 2.829673582, \quad b_1 = 3.528046148, \quad a_2 = 1.902891314, \quad b_2 = 1.161374634, \quad (4.37)$$

or the equivalent solution with $a_1 \Leftrightarrow a_2$ and $b_1 \Leftrightarrow b_2$.

The corresponding prediction for the muon anomaly is

$$a_\mu^{\text{VP}}(N=4) = \left(\frac{\alpha}{\pi}\right)^3 0.0528711, \quad (4.38)$$

which reproduces the exact value at the level of 0.00075%, practically the exact result.

It seems fair to conclude from these examples that the successive use of MBa of the Marichev class in Eq. (3.30) is an excellent method to approach, rather quickly in this case, the exact result with an excellent accuracy. The question which, however, arises is: *how far can one go?*. The exact Mellin transform of the QED fourth order spectral function, contrary to the second order one which we discussed earlier, is expected to be a much more complicated expression than just a simple *standard product* of the Marichev class in Eq. (3.30). Therefore, one normally expects that these approximations should break at some N -level. Let us then proceed to examine what happens when one tries higher N -MBa's of this type.

IV.1.5 The $N = 5$ MBa.

The $N = 5$ Mellin approximant is

$$\mathcal{M}_{4\text{th}}^{\text{QED}}(s) \Rightarrow \mathcal{M}_5(s) = C_5 \frac{\Gamma(1-s)\Gamma(a_1-s)\Gamma(a_2-s)}{\Gamma(b_1-s)\Gamma(b_2-s)\Gamma(b_3-s)}, \quad (4.39)$$

with

$$C_5 = \left(\frac{\alpha}{\pi}\right)^2 \frac{1}{4} \frac{\Gamma(b_1 - 1)\Gamma(b_2 - 1)\Gamma(b_3 - 1)}{\Gamma(a_1 - 1)\Gamma(a_2 - 1)}, \quad (4.40)$$

and the parameters a_1, a_2, b_1, b_2, b_3 solutions of the matching equations:

$$\frac{1}{4} \frac{a_1 - 1}{b_1 - 1} \frac{a_2 - 1}{b_2 - 1} \frac{1}{b_3 - 1} = \mathcal{M}_{4\text{th}}^{\text{QED}}(0), \quad (4.41)$$

$$\frac{a_1}{b_1} \frac{a_2}{b_2} \frac{1}{b_3} = \frac{\mathcal{M}_{4\text{th}}^{\text{QED}}(-1)}{\mathcal{M}_{4\text{th}}^{\text{QED}}(0)}, \quad (4.42)$$

$$2 \frac{a_1 + 1}{b_1 + 1} \frac{a_2 + 1}{b_2 + 1} \frac{1}{b_3 + 1} = \frac{\mathcal{M}_{4\text{th}}^{\text{QED}}(-2)}{\mathcal{M}_{4\text{th}}^{\text{QED}}(-1)}, \quad (4.43)$$

$$3 \frac{a_1 + 2}{b_1 + 2} \frac{a_2 + 2}{b_2 + 2} \frac{1}{b_3 + 2} = \frac{\mathcal{M}_{4\text{th}}^{\text{QED}}(-3)}{\mathcal{M}_{4\text{th}}^{\text{QED}}(-2)}, \quad (4.44)$$

$$4 \frac{a_1 + 3}{b_1 + 3} \frac{a_2 + 3}{b_2 + 3} \frac{1}{b_3 + 3} = \frac{\mathcal{M}_{4\text{th}}^{\text{QED}}(-4)}{\mathcal{M}_{4\text{th}}^{\text{QED}}(-3)}, \quad (4.45)$$

with solution values:

$$b_1 = 1.16249580, a_1 = 4.111523616, b_2 = 4.354959443, a_2 = 2.360299888, b_3 = 2.917297589, \quad (4.46)$$

and other equivalent solutions permutations of a_1, a_2 and b_1, b_2, b_3 .

The corresponding prediction for the muon anomaly is now

$$a_\mu^{\text{VP}}(N = 5) = \left(\frac{\alpha}{\pi}\right)^3 0.0528706, \quad (4.47)$$

which reproduces the exact value at the level of 0.00018%, still an improvement with respect to the $N = 4$ Approximation! This is, however, the best one can do in the two loop QED case with Mellin approximants of the type shown in Eq. (3.30). Indeed, if one tries to improve with a $N = 6$ MBa of this type, one finds that all the solutions for the parameters $a_1, a_2, a_3, b_1, b_2, b_3$ from the matching equations bring in complex numbers with real parts which are inside of the *fundamental strip*, in contradiction with the initial requirements for an acceptable solution that we imposed. This is the signal that the method of simple Marichev-like approximants that we are using breaks down at that level. It breaks down because, beyond a certain level of accuracy, the function $\Pi_{4\text{th}}^{\text{QED}}(Q^2)$ cannot be approximated by just one GH-Function. It is possible, however, as we shall next discuss in the QCD case, to improve on the class of Marichev-like approximants introducing *superpositions of standard products* of gamma functions.

From the previous analysis we conclude that, in the case of the QED fourth order vacuum polarization, the best prediction we can make with simple Marichev-like MBa's is an average of the $N = 4$ and $N = 5$ approximants with an error estimated from the deviation of this average to the $N = 4$ and $N = 5$ results i.e.,

$$a_\mu^{\text{VP}}(\text{QED 4th order}) = \left(\frac{\alpha}{\pi}\right)^3 (0.0528709 \pm 0.0000003). \quad (4.48)$$

This is already an excellent prediction when compared to the exact result in Eq. (4.7).

v Test of MBa with experimental HVP Moments.

The KNT collaboration [9] has kindly provided us with preliminary values of the first few moments of the hadronic spectral function with errors, as well as their covariance matrix. These results provide a good test of how well the MBa method that we propose works when applied to a set of moments with realistic errors.

The first five moments with their errors are given in Table (2) and their correlation matrix is given in Table (3) in the next section. We observe that the relative errors of the first two moments $\mathcal{M}(0)$ and $\mathcal{M}(-1)$ in Table (2) are smaller than the relative error in the determination of the lowest order HVP contribution to a_μ^{HVP} in Eq. (1.3) [9]. The higher moments $\mathcal{M}(-n)$ for $n = 2, 3, \dots$ have higher relative errors but they of course contribute less and less to the total a_μ^{HVP} determination.

Table 2: $\mathcal{M}(s)$ Moments and Errors in 10^{-3} units .

Moment	Experimental Value	Relative Error
$\mathcal{M}(0)$	0.7176 ± 0.0026	0.36%
$\mathcal{M}(-1)$	0.11644 ± 0.00063	0.54%
$\mathcal{M}(-2)$	0.03041 ± 0.00029	0.95%
$\mathcal{M}(-3)$	0.01195 ± 0.00017	1.4%
$\mathcal{M}(-4)$	0.00625 ± 0.00011	1.8%
$\mathcal{M}(-5)$	0.003859 ± 0.000078	2.0%

We shall next proceed, like in the previous section, to the construction of successive MBa's of the type shown in Eq. (3.30) and to the evaluation of the corresponding GH-Functions $\Pi_N^{\text{QCD}}(Q^2)$ and $\frac{1}{\pi}\text{Im}\Pi_N(t)$. At each approximation we shall then evaluate the corresponding $a_\mu^{\text{HVP}}(N)$ contribution to the muon anomaly. Here we shall only consider as input the center values of the moments in Table (2) and postpone the error analysis for later discussion in the next subsection.

V.1 Successive MBa's to $\mathcal{M}^{\text{QCD}}(s)$, $\Pi^{\text{QCD}}(Q^2)$, $\frac{1}{\pi}\text{Im}\Pi^{\text{QCD}}(t)$ and a_μ^{HVP} .

V.1.1 The $N = 1$ MBa.

This corresponds to the MBa which one can construct when only the first moment $\mathcal{M}(0)$ is known. In this case

$$\mathcal{M}_1(s) = \frac{\alpha}{\pi} \frac{5}{3} \Gamma(1-s) \frac{\Gamma(b_1-1)}{\Gamma(b_1-s)}, \quad (5.1)$$

where the singularity at $s = 1$ is the one associated to the asymptotic leading behaviour of the QCD spectral function with u, d, s, c, b and t quarks in Eq. (2.1). Matching the value of $\mathcal{M}_1(s)$ at $s = 0$ with the one from the experimental determination in Table (2) fixes the b_1 -parameter to the value:

$$b_1 = 6.395. \quad (5.2)$$

Figure (16) shows the shape of the predicted Mellin transform. The blue points in the figure correspond to the experimental values of the moments in Table (2) with their errors, which are too small to be seen at the scale in the figure. The agreement, at the precision of the scale of the figure, is excellent.

Inserting the expression of the first Mellin approximant $\mathcal{M}_1(s)$ in the integrand at the r.h.s. of Eq. (2.15) gives the result of the first MBa to the muon anomaly:

$$a_\mu^{\text{HVP}}(N=1) = \left(\frac{\alpha}{\pi}\right) \sqrt{\frac{m_\mu^2}{t_0}} \frac{1}{2\pi} \int_{-\infty}^{+\infty} d\tau e^{i\tau \log \frac{m_\mu^2}{t_0}} \mathcal{F}\left(\frac{1}{2} - i\tau\right) \mathcal{M}_{N=1}\left(\frac{1}{2} - i\tau\right) \quad (5.3)$$

$$= 6.991 \times 10^{-8}, \quad (5.4)$$

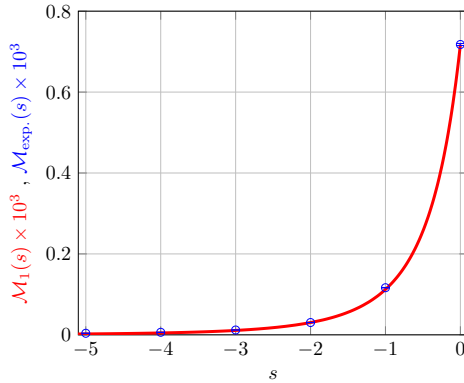


Figure 16:

The red curve shows the shape of the $N = 1$ MBA in Eq. (5.1).
The blue circles are the experimental values in Table (2).

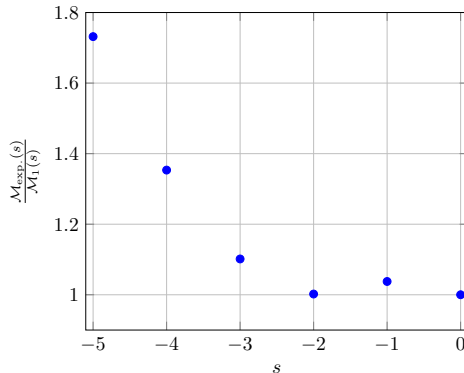


Figure 17:

Plot of the ratio of the experimental moments in Table (2) with their errors to those predicted by the $N = 1$ Mellin-Barnes-Approximation.

which reproduces the central value result in Eq. (1.3) [9] surprisingly well: to 0.8%.

In order to understand why the $N = 1$ MBA is already so good, let us explore more in detail the plot of $\mathcal{M}_1(s)$ in Fig (16). To better observe the deviations between the experimental moments and the predicted moments we plot in Fig. (17) their ratio as a function of $s = -n$, $n = 0, 1, 2, \dots$. The deviation of this ratio from one shows the discrepancy. Notice that, here, only the value of the $\mathcal{M}(0)$ moment has been used as an input. The predicted values of $\mathcal{M}(-1)$, $\mathcal{M}(-2)$ and even $\mathcal{M}(-3)$ turn out to be rather close to the experimental values, although already the predicted $\mathcal{M}(-3)$ and certainly the predicted higher moments are not compatible with the experimental statistical errors. Higher moments, however, contribute less and less to the total value of the anomaly and this is why $a_\mu^{\text{HVP}}(N = 1)$ turns out to be such a good approximation.

Why does the $N = 1$ MBA do a better job in the case of QCD than in the two loop QED case we discussed before? The reason for this is that in the QCD case, contrary to the QED case, there are resonances in the low energy region of the spectral function with mass scales which, relative to the muon mass, enhance the contribution of the low moments, in particular $\mathcal{M}(0)$. If instead of the muon anomaly we were considering the electron anomaly, the $N = 1$ MBA would already be giving a result with an accuracy comparable to the full determination.

Although, given the result in Eq. (5.3) and the present accuracy from experiment, there seems to be little room for improvement, let us examine what happens when one tries the $N = 2$ MBa.

V.1.2 The $N = 2$ MBa.

Here the Mellin approximant has the analytic form

$$\mathcal{M}_2(s) = \frac{\alpha}{\pi} \frac{5}{3} \frac{\Gamma(1-s) \Gamma(a_1-s) \Gamma(b_1-1)}{\Gamma(2-s) \Gamma(a_1-1) \Gamma(b_1-s)}, \quad (5.5)$$

and the parameters a_1 and b_1 are fixed by the matching equations:

$$\mathcal{M}_2(0) = \mathcal{M}(0) \quad \text{and} \quad \mathcal{M}_2(-1) = \mathcal{M}(-1), \quad (5.6)$$

with $\mathcal{M}(0)$ and $\mathcal{M}(-1)$ given in Table (2). This results in the values:

$$a_1 = 1.900 \quad \text{and} \quad b_1 = 5.855. \quad (5.7)$$

The shape of the $\mathcal{M}_2(s)$ Mellin transform turns out to be rather similar to the $\mathcal{M}_1(s)$ one in Fig. (17). In order to appreciate the differences between the $N = 1$ and $N = 2$ MBa's, we compare in Fig. (18) the ratios of the experimental moments to those of the $\mathcal{M}_2(s)$ prediction (the red dots) and to those of the $\mathcal{M}_1(s)$ prediction (the blue dots). The overall shape of the red dots is clearly better because they are nearer to one.

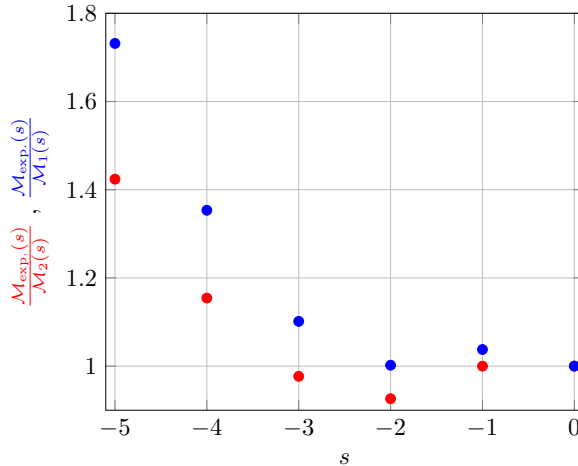


Figure 18:

Plot of the ratio of the experimental moments in Table (2) with their errors to those predicted by the $N = 2$ MBa in red and the $N = 1$ MBa in blue.

With the expression of the second Mellin approximant $\mathcal{M}_2(s)$ inserted in the integrand at the r.h.s. of Eq. (2.15) we get as a result of the $N = 2$ MBa to the muon anomaly:

$$a_\mu^{\text{HVP}}(N=2) = \left(\frac{\alpha}{\pi}\right) \sqrt{\frac{m_\mu^2}{t_0}} \frac{1}{2\pi} \int_{-\infty}^{+\infty} d\tau \underbrace{e^{i\tau \log \frac{m_\mu^2}{t_0}} \mathcal{F}\left(\frac{1}{2} - i\tau\right) \mathcal{M}_{N=2}\left(\frac{1}{2} - i\tau\right)}_{\mathcal{R}(\tau)} \quad (5.8)$$

$$= 6.970 \times 10^{-8}, \quad (5.9)$$

which reproduces the central value result in Eq. (1.3) [9] at the 0.5% level, i.e. an improvement by a factor of 1.6 with respect to the $N = 1$ case. Figure (19) shows the shape of the integrand $\mathcal{R}(\tau)$ in Eq. (5.8) which, as expected, has a rapid decrease as $|\tau| \gtrsim 1$.

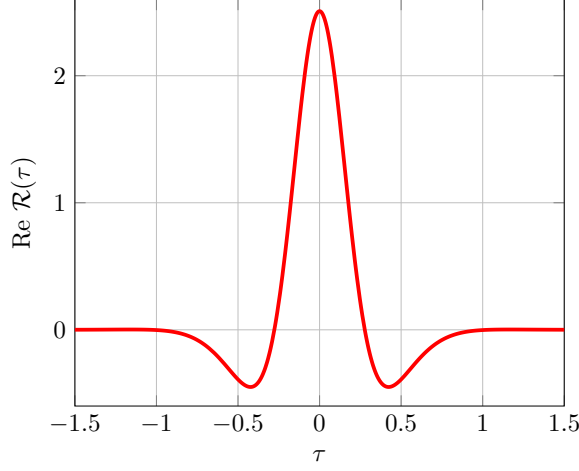


Figure 19:

Plot of the integrand in Eq. (5.8) as a function of τ .

As discussed in the previous section, the MBa technique allows to reconstruct as well $\Pi_N(Q^2)$ approximants of the HVP self energy in terms of GH-functions. The corresponding $N = 2$ approximant is ($z = \frac{Q^2}{t_0}$):

$$\Pi_{N=2}^{\text{QCD}}(Q^2) = \left(\frac{\alpha}{\pi}\right) (-z) \frac{5}{3} \frac{a_1 - 1}{b_1 - 1} {}_3F_2 \left(\begin{matrix} 1 & 1 & a_1 \\ 2 & b_1 \end{matrix} \middle| -z \right), \quad (5.10)$$

with a_1 and b_1 given in Eq. (5.7). The shape of the function $\Pi_{N=2}^{\text{QCD}}(Q^2)$ is shown in Fig. (20).

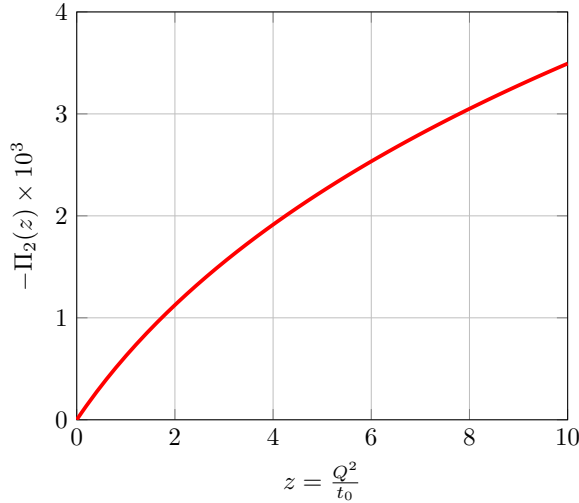


Figure 20:

Shape of the function $\Pi_{N=2}^{\text{QCD}}(Q^2)$ in Eq. (5.10) as a function of $z = \frac{Q^2}{t_0}$.

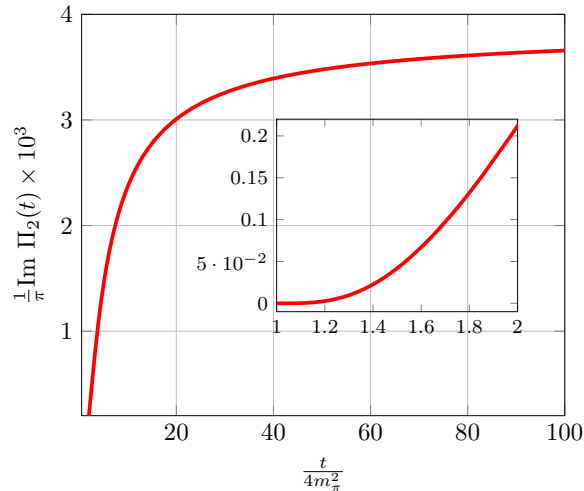


Figure 21:

Plots of the $N = 2$ MBa Spectral Function.

Plots of the spectral function associated to the $N = 2$ MBa are also shown in Figs.(21). Although, asymptotically, the $N = 2$ MBa spectral function approaches the pQCD value it can only be considered a smooth interpolation of the physical spectral function which, as we know, has a lot of local structure. This interpolation, however, when inserted in the r.h.s. of Eq. (1.4) reproduces the determination of the anomaly using the experimental spectral function at the 0.5% level already mentioned. It is in this sense that it is a good interpolation.

We shall next explore what happens when one tries to improve the $N = 2$ MBa with higher approximants and further input from the experimental values of higher moments.

V.1.3 The $N = 3$ MBa.

The corresponding Mellin approximant which generalizes the one in Eq. (5.1) has the analytic form

$$\mathcal{M}_3(s) = \frac{\alpha}{\pi} \frac{5}{3} \Gamma(1-s) \frac{\Gamma(b_1-1) \Gamma(a_1-s) \Gamma(b_2-1)}{\Gamma(b_1-s) \Gamma(a_1-1) \Gamma(b_2-s)}, \quad (5.11)$$

with the parameters a_1 , b_1 and b_2 solutions of the matching equations

$$\mathcal{M}_3(0) = \mathcal{M}(0), \quad \mathcal{M}_3(-1) = \mathcal{M}(-1) \quad \text{and} \quad \mathcal{M}_3(-2) = \mathcal{M}(-2). \quad (5.12)$$

In this case one finds a “possible solution” where

$$a_1 = -0.362, \quad b_1 = 6.462, \quad b_2 = -0.346, \quad (5.13)$$

and the equivalent one with $b_1 \rightleftharpoons b_2$. These “solutions”, however, are not acceptable because they generate a pole at $s = a_1$ which is inside of the fundamental strip in contradiction with first principles, as discussed in Section III.3. Nevertheless, the negative numerical values of a_1 and b_2 are in fact rather close to each other. Had they been exactly the same, there would have been a cancellation between $\Gamma(a_1 - s)$ and $\Gamma(b_2 - s)$ in Eq. (5.11) indicating that it is not possible to improve beyond $N = 2$ with a single Marichev-like function. The situation here is rather similar to the one encountered earlier when considering the $N = 6$ MBa in the QED example.

The fact that in QCD the simple Marichev-like approximants fail to find physical solutions already at the $N = 3$ level is perhaps not so surprising. One does not expect, beyond a certain level of accuracy,

to be able to approximate $\Pi^{\text{QCD}}(Q^2)$ at all Q^2 values with just one GH-function. One may, however, ask: is it possible to find generalizations of the simple Marichev-like MBa's which, when using more than the first two moments in Table (2) as an input, provide acceptable solutions to compare with a_μ^{HVP} in Eq. (1.3) [9]? There is a positive answer to that, as we shall next discuss. It consists in using superpositions of Mellin approximants of the Marichev type. This, in turn, implies specific superpositions of GH-Functions which approximate the self-energy $\Pi^{\text{QCD}}(Q^2)$ in the Euclidean, and hence a_μ^{HVP} .

V.1.4 The $N = (2) + (1)$ MBa.

The simplest superposition which gives acceptable solutions to the matching equations, when one knows three moments, is the one which consists of the sum of one $N = 2$ MBa and one $N = 1$ MBa, with the correct pQCD behaviour at $s = 1$ (hence the overall factor $1/2$), i.e.

$$\mathcal{M}_{2+1}(s) = \frac{\alpha}{\pi} \frac{5}{3} \frac{1}{2} \left\{ \frac{1}{1-s} \frac{\Gamma(a_1-s)}{\Gamma(a_1-1)} \frac{\Gamma(b_1-1)}{\Gamma(b_1-s)} + \Gamma(1-s) \frac{\Gamma(b_2-1)}{\Gamma(b_2-s)} \right\}, \quad (5.14)$$

and the parameters a_1 , b_1 and b_2 solutions of the matching equations:

$$\mathcal{M}_{2+1}(0) = \mathcal{M}(0), \quad \mathcal{M}_{2+1}(-1) = \mathcal{M}(-1) \quad \text{and} \quad \mathcal{M}_{2+1}(-2) = \mathcal{M}(-2). \quad (5.15)$$

There is only one acceptable solution to these equations with the values:

$$a_1 = 5.2668, \quad b_1 = 14.514, \quad \text{and} \quad b_2 = 19.177. \quad (5.16)$$

With $\mathcal{M}_{2+1}(s)$ inserted in the integrand at the r.h.s. of Eq. (2.15) we get as a result for the muon anomaly:

$$a_\mu^{\text{HVP}}(N = 2 + 1) = 6.957 \times 10^{-8} \quad (5.17)$$

which reproduces the central value result in Eq. (1.3) [9] at the 0.4% level, and is an improvement with respect to the $N = 2$ case.

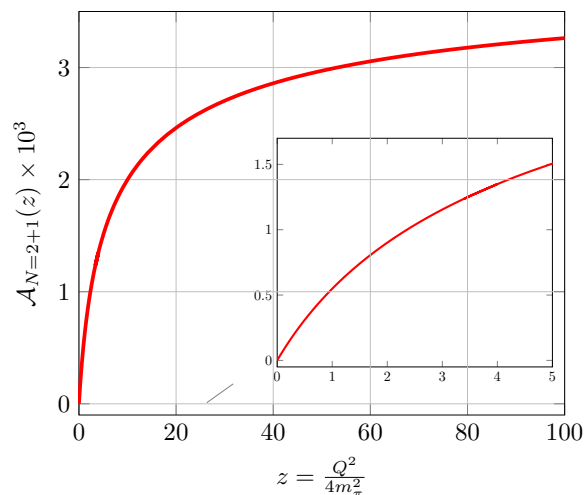


Figure 22:

Plots of the $N = 2 + 1$ Adler Function versus $z = \frac{Q^2}{t_0}$.

The corresponding sum of HG-Functions to the $\mathcal{M}_{2+1}(s)$ MBa in Eq. (5.15) which results as an approximation to the HVP self-energy is now

$$\begin{aligned} \Pi_{N=2+1}^{\text{QCD}}(Q^2) = \left(\frac{\alpha}{\pi}\right) (-z) \frac{5}{3} \frac{1}{2} \left\{ \frac{a_1-1}{b_1-1} {}_3F_2 \left(\begin{matrix} 1 & 1 & a_1 \\ & 2 & b_1 \end{matrix} \middle| -z \right) \right. \\ \left. + \frac{1}{b_2-1} {}_2F_1 \left(\begin{matrix} 1 & 1 \\ & b_2 \end{matrix} \middle| -z \right) \right\}, \end{aligned} \quad (5.18)$$

and the corresponding approximation to the Adler function is

$$\begin{aligned} \mathcal{A}_{N=2+1}^{\text{QCD}}(Q^2) = \left(\frac{\alpha}{\pi}\right) z \frac{5}{3} \frac{1}{2} \left\{ \frac{a_1-1}{b_1-1} {}_3F_2 \left(\begin{matrix} 2 & 1 & a_1 \\ & 2 & b_1 \end{matrix} \middle| -z \right) \right. \\ \left. + \frac{1}{b_2-1} {}_2F_1 \left(\begin{matrix} 2 & 1 \\ & b_2 \end{matrix} \middle| -z \right) \right\}. \end{aligned} \quad (5.19)$$

The shape of this Adler function is shown in Fig. (22).

V.1.5 The $N = (2) + (1) + (1)$ MBa.

With the first four moments as an input, there is a new superposition of MBa's which gives an acceptable solution to the matching equations. It is the following linear combination of a $N = 2$ MBa and two $N = 1$ MBa's:

$$\mathcal{M}_{2+1+1}(s) = \frac{\alpha}{\pi} \frac{5}{3} \left\{ \frac{1}{1-s} \frac{\Gamma(a_1-s)\Gamma(b_1-1)}{\Gamma(a_1-1)\Gamma(b_1-s)} + \Gamma(2-s) \frac{\Gamma(b_2-1)}{\Gamma(b_2-s)} + \Gamma(2-s) \frac{\Gamma(b_3-1)}{\Gamma(b_3-s)} \right\}. \quad (5.20)$$

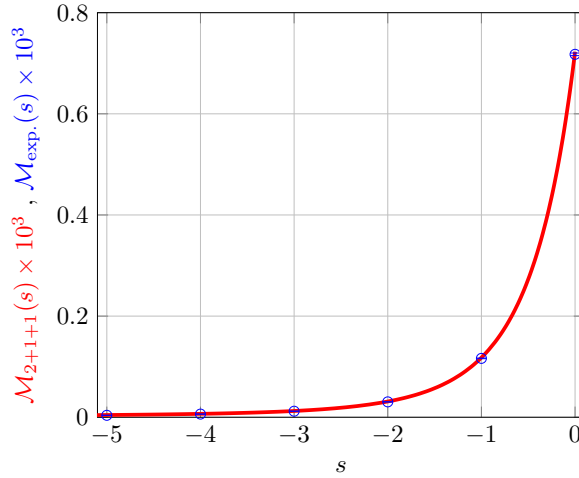


Figure 23:

The red curve is the shape of \mathcal{M}_{2+1+1} in Eq. (5.20) for $-5 \leq s \leq 0$.
The dots are the experimental values of the moments.

The matching equations:

$$\begin{aligned} \mathcal{M}_{2+1+1}(0) = \mathcal{M}(0), \quad \mathcal{M}_{2+1+1}(-1) = \mathcal{M}(-1), \\ \mathcal{M}_{2+1+1}(-2) = \mathcal{M}(-2), \quad \text{and} \quad \mathcal{M}_{2+1+1}(-3) = \mathcal{M}(-3), \end{aligned} \quad (5.21)$$

give an acceptable solution with values:

$$a_1 = 1.0190, \quad b_1 = 1.7495, \quad (5.22)$$

and two complex conjugate values for b_2 and b_3 , or equivalently $b_2 = b_3^*$:

$$b_2 = 12.822 + i 2.6069, \quad b_3 = 12.822 - i 2.6069, \quad (5.23)$$

which gives a total real contribution to the sum of the two $N = 1$ terms in Eq. (5.20).

The expression of the $N = 2 + 1 + 1$ Mellin approximant $\mathcal{M}_{2+1+1}(s)$ inserted in the integrand at the r.h.s. of Eq. (2.15) results in a value for the muon anomaly:

$$a_\mu^{\text{HVP}}(N = 2 + 1 + 1) = 6.932 \times 10^{-8}, \quad (5.24)$$

which almost exactly reproduces the central value result in Eq. (1.3) [9], and represents a net improvement with respect to the previous $N = 2 + 1$ approximation.

The shape of the Mellin transform $\mathcal{M}_{2+1+1}(s)$ is shown in Fig. (23) together with the experimental values of the first five moments. Figure (24) shows the ratio of the experimental values of the first five moments to the values predicted by \mathcal{M}_{2+1+1} in Eq. (5.20).

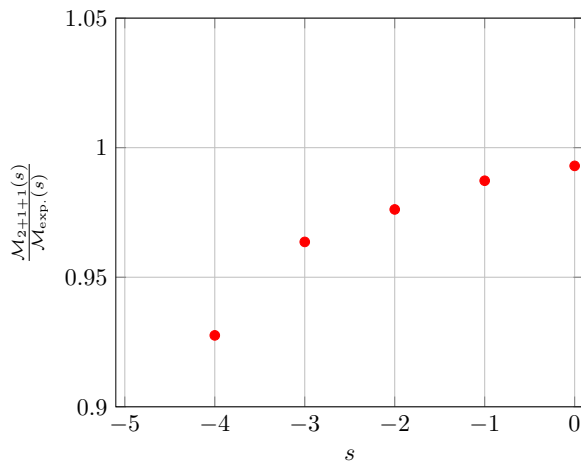


Figure 24:

Plot of the ratio of the experimental moments in Table (2) to those of the $N = 2 + 1 + 1$ MBa.

The Adler function associated to $\mathcal{M}_{2+1+1}(s)$ in Eq. (5.20) is the sum of three GH-Functions:

$$\begin{aligned} \mathcal{A}_{N=2+1+1}^{\text{QCD}}(Q^2) = & \left(\frac{\alpha}{\pi}\right) z \frac{5}{3} \left\{ \frac{a_1 - 1}{b_1 - 1} {}_3F_2 \left(\begin{matrix} 2 & 1 & a_1 \\ & 2 & b_1 \end{matrix} \middle| -z \right) \right. \\ & \left. + \frac{1}{b_2 - 1} {}_2F_1 \left(\begin{matrix} 2 & 2 \\ & b_2 \end{matrix} \middle| -z \right) + \frac{1}{b_3 - 1} {}_2F_1 \left(\begin{matrix} 2 & 2 \\ & b_3 \end{matrix} \middle| -z \right) \right\}, \quad (5.25) \end{aligned}$$

and its shape is shown in Fig. (25).

Plots of the spectral function corresponding to the $N = 2 + 1 + 1$ MBa are also shown in Fig. (26). The plots already exhibit underlying features of the hadronic structure.

V.2 Uncertainties of the Successive MBa's to a_μ^{HVP} .

We shall finally examine the sensitivity of the results obtained for the $a_\mu^{\text{HVP}}(N)$ to small variations in the input parameters a_k and b_k of the successive $\mathcal{M}_N(s)$, as well as to the choice of the N -approximant itself. The errors in the experimental determination of the moments $\mathcal{M}(-n)$ have been

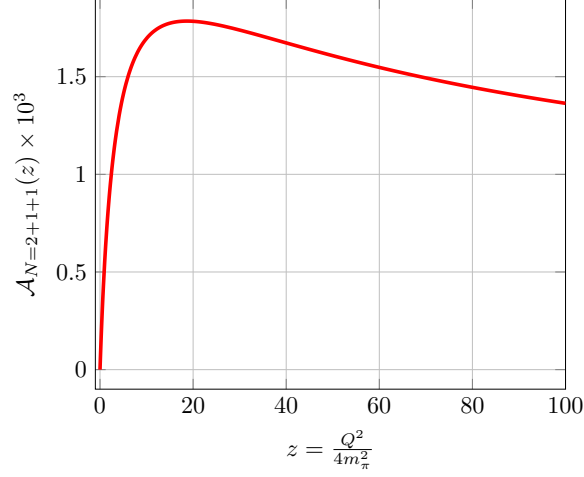


Figure 25:

Plot of the Adler function in Eq. (5.25).

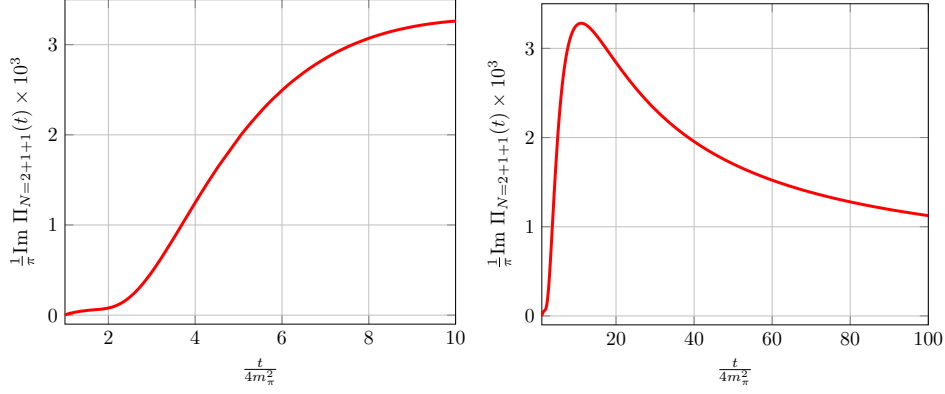


Figure 26:

Plots of the $N = 2 + 1 + 1$ Spectral Function.

tabulated in Table (2) and their correlation matrix is given in Table (3). One can see that the values of these moments are highly correlated, reflecting the fact that they all have been extracted from different integrals of the same input data on the spectral function.

The statistical part of the analysis is standard. We first construct the covariance matrix C_{ij} of the first N moments obtained from experiment $\mathcal{M}(1-i)$, $i = 1, \dots, N$:

$$C_{ij} = \rho_{ij} \sigma_i \sigma_j, \quad \text{with } \rho_{ii} = 1, \quad -1 < \rho_{i,j} < +1 \quad \text{and } i, j = 1, \dots, N, \quad (5.26)$$

where ρ_{ij} is the correlation coefficient between the moment $\#i$ and the moment $\#j$, each with Gaussian uncertainty σ_i and σ_j . Then we define a χ^2 function associated to a given Mellin-Barnes approximant $\mathcal{M}_N(s)$, which depends on a set of parameters (a_k, b_k) :

$$\chi^2 = \sum_{i,j=1}^N [\mathcal{M}_N(1-i) - \mathcal{M}(1-i)] C_{ij}^{-1} [\mathcal{M}_N(1-j) - \mathcal{M}(1-j)]. \quad (5.27)$$

and minimize this χ^2 with respect to the set of parameters (a_k, b_k) . The errors are sufficiently small to ensure that a point-like estimate is an excellent approximation, and we obtain the covariance matrix

Table 3: *Correlation Matrix of the Moments $\mathcal{M}(0), \dots, \mathcal{M}(-5)$ in Table (2)*

$$\begin{pmatrix} 1 & 0.83 & 0.62 & 0.50 & 0.42 & 0.37 \\ & 1 & 0.93 & 0.84 & 0.77 & 0.70 \\ & & 1 & 0.98 & 0.93 & 0.88 \\ & & & 1 & 0.987 & 0.96 \\ & & & & 1 & 0.991 \\ & & & & & 1 \end{pmatrix}.$$

in the (a_k, b_k) parameter space from the Hessian matrix of the χ^2 function computed at its minimum. Using linear error propagation we can then calculate the statistical uncertainty on a_μ^{HVP} , as reported in the third column of Table (4). The fact that all the approximants have a similar uncertainty that coincides with the one of the complete evaluation of a_μ^{HVP} [9] is a sign that the statistical information is saturated by all our MBa's.

Table 4: Numerical results on the determination of a_μ^{HVP} (10^{-8} units), for each considered MBa.

MBa Ansatz	Central Value	Stat. Uncertainty
Eq. (5.1) ($N = 1$)	6.991	0.023
Eq. (5.5) ($N = 2$)	6.970	0.024
Eq. (5.14) ($N = (2) + (1)$)	6.957	0.025
Eq. (5.20) ($N = (2) + (1) + (1)$)	6.932	0.025

Our results would not be complete without a study of the systematic shift associated to the successive MBa's which interpolate the values of the experimental moments and reconstruct the full Mellin functions. With this aim, in addition to the MBa's discussed in detail in the previous section, we have also tested alternative parameterizations for $N = 2, 3, 4$ which are obtained by changing the location of the poles in the superposition terms (*e.g.* $\Gamma(2-s)$ instead of $\Gamma(1-s)$ in Eq. (5.14)). These alternative MBa's have also valid solutions for the corresponding (a_k, b_k) parameters and, therefore, can also be considered as good alternative choices. The results of all the evaluations of a_μ^{HVP} which we have made are plotted in Fig. (27), as a function of the number of input moments N . We observe that the successive results converge towards the experimental value in Eq. (1.3).

VI Conclusions and Outlook

Equation (2.3) shows that moments of the hadronic spectral function are equivalent to derivatives of the hadronic self-energy function $\Pi(Q^2)$ at $Q^2 = 0$. The latter are accessible to LQCD simulations as well as to eventual dedicated experiments. We have shown how, from an accurate determination of the first few moments, one could reach an evaluation of the HVP contribution to the muon anomaly with a competitive precision, or even higher, than the present experimental determinations.

The method that we propose uses a new technique of Mellin-Barnes approximants which has been explained and justified in detail in the text. Essentially it is based on generic QCD properties which fix the class of Mellin transforms $\mathcal{M}(s)$ of the spectral function that one can use as successive approximants. The muon anomaly a_μ^{HVP} , in terms of these $\mathcal{M}(s)$ -functions, is given by the Fourier transform in Eq. (2.20). The corresponding approximations to the hadronic self-energy function $\Pi(Q^2)$ are well defined Generalized Hypergeometric Functions which we have given explicitly and the approximations to the spectral function are also given in terms of Meijer's G-Functions. This offers the possibility of applying the same techniques developed here to the case where the information from LQCD, or from experiment, is given in terms of determinations of the self-energy function $\Pi(Q^2)$ at fixed Euclidean Q^2 -values, as *e.g.* in ref. [16]. We plan to discuss this in the near future.

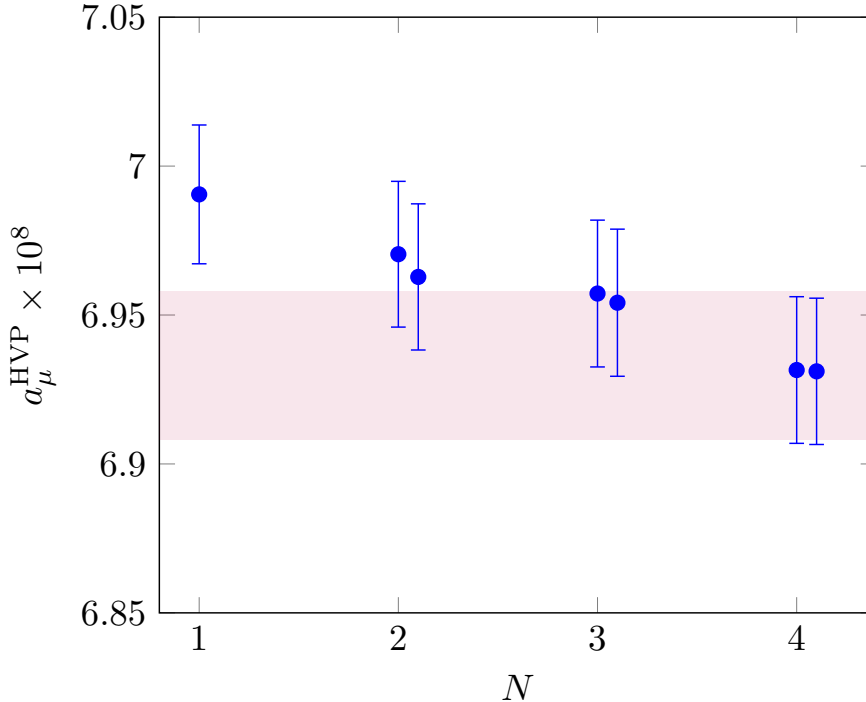


Figure 27:

Results for a_μ^{HVP} as a function of the number of input moments N . The blue points correspond to alternative choices of MBa's (two choices for $N = 2, 3, 4$) with their statistical uncertainty. The pink band is the full experimental result of ref. [9].

We have illustrated the practical application of the method with the example of the QED contribution to the muon anomaly from the vacuum polarization Feynman diagrams in Fig. (8). We have also discussed the case where one uses as an input the experimental values of the first moments provided to us by the collaboration of ref. [9]. We find that, in this case, our approach reproduces very well their complete phenomenological analysis.

Acknowledgments

We are very grateful to Thomas Teubner and to Alex Keshavarzi for providing us with the experimental preliminary values of the first few moments and the error correlations of their update. We also thank Laurent Lellouch and Ruth Van de Water for their interest and informative discussions, and Alex Keshavarzi and Ruth Van de Water for a careful reading of the manuscript. D.G. thanks M. Knecht and CPT for their hospitality during the beginning of this work.

This work has been carried out thanks to the support of the OCEVU Labex (ANR-11-LABX-0060) and the A*MIDEX project (ANR-11-IDEX-0001-02) funded by the "Investissements d'Avenir" French government program managed by the ANR.

APPENDIX

In this appendix we discuss various technical details which appear in the main text

A The Basic Mellin-Barnes Identity

The identity in Eq. (2.10) is a particular case of the identity ($N = 1, 2, 3, \dots$):

$$\frac{1}{(1+A)^N} = \frac{1}{2\pi i} \int_{c_s - i\infty}^{c_s + i\infty} ds (A)^{-s} \frac{\Gamma(s)\Gamma(N-s)}{\Gamma(N)}. \quad (\text{A.1})$$

We shall first show how performing the integral in the r.h.s. for $N = 1$ reproduces the l.h.s. For that we make a choice of s with $\text{Re}(s) \in]0, 1[$, e.g. $s = \frac{1}{2} + i\tau$. Then

$$\begin{aligned} & \frac{1}{2\pi i} \int_{c_s - i\infty}^{c_s + i\infty} ds (A)^{-s} \Gamma(s)\Gamma(1-s) \\ &= \frac{1}{\sqrt{A}} \frac{1}{2\pi} \int_{-\infty}^{+\infty} d\tau \exp(-i\tau \log A) \frac{\pi}{\cosh(\pi\tau)} \\ &= \frac{1}{\sqrt{A}} \frac{1}{2\pi} \frac{\pi}{\cosh\left(\frac{\log A}{2}\right)} = \frac{1}{\sqrt{A}} \frac{1}{2} \frac{1}{e^{\frac{1}{2}\log A} + e^{-\frac{1}{2}\log A}} \\ &= \frac{1}{\sqrt{A}} \frac{1}{\sqrt{A} + \frac{1}{\sqrt{A}}} = \frac{1}{1+A}, \quad \text{c.q.d.} \end{aligned} \quad (\text{A.2})$$

Taking N -derivatives with respect to A in this identity reproduces Eq. (A.1).

We shall next evaluate the Mellin transform of $\frac{1}{(1+A)^N}$ and show that

$$\int_0^\infty dA A^{s-1} \frac{1}{(1+A)^N} = \frac{\Gamma(s)\Gamma(N-s)}{\Gamma(N)}. \quad (\text{A.3})$$

We do that by applying Ramanujan's Master Theorem to the Taylor expansion:

$$\frac{1}{(1+A)^N} = \sum_{k=0,1,2,\dots} (-1)^k \left[\frac{\Gamma(N+k)}{\Gamma(N)\Gamma(k+1)} \right] A^k, \quad (\text{A.4})$$

from which Ramanujan allows us to conclude that

$$\int_0^\infty dA A^{s-1} \frac{1}{(1+A)^N} = \Gamma(s)\Gamma(1-s) \times \left[\frac{\Gamma(N-s)}{\Gamma(N)\Gamma(-s+1)} \right] \quad (\text{A.5})$$

$$= \frac{\Gamma(s)\Gamma(N-s)}{\Gamma(N)}, \quad \text{c.q.d.} \quad (\text{A.6})$$

B Positivity Properties of the Mellin Moments

Because of the positivity property of the spectral function $\frac{1}{\pi}\text{Im}\Pi(t)$ the Mellin Moments $\mathcal{M}(-N)$ which, here, for convenience, we write as follows

$$\Sigma(N) = \int_{t_0}^\infty \frac{dt}{t_0} \left(\frac{t_0}{t} \right)^{2+N} \frac{1}{\pi} \text{Im}\Pi(t), \quad N = 0, 1, 2, \dots, \quad (\text{B.1})$$

must satisfy certain constraints which we next discuss. Notice that with this definition:

$$\mathcal{M}(-n) \equiv \Sigma(N = n). \quad (\text{B.2})$$

It is useful to change variables slightly: set

$$z = \frac{t_0}{t}, \quad \frac{dt}{t_0} = -\frac{dz}{z^2}, \quad (\text{B.3})$$

and, therefore,

$$\Sigma(N) = \int_0^1 dz z^N \frac{1}{\pi} \text{Im} \Pi \left(\frac{1}{z} t_0 \right). \quad (\text{B.4})$$

The positivity constraints follow from the fact that

$$\sum_{N, N'} \left[\int_0^1 dz z^{N+N'} \frac{1}{\pi} \text{Im} \Pi \left(\frac{1}{z} t_0 \right) \right] \xi_N \xi'_N \geq 0, \quad (\text{B.5})$$

where ξ_N and ξ'_N are the components of arbitrary positive real vectors. This implies that the matrix

$$\Sigma(N, N') \equiv \int_0^1 dz z^{N+N'} \frac{1}{\pi} \text{Im} \Pi \left(\frac{1}{z} t_0 \right), \quad (\text{B.6})$$

must be positive definite. The relevant constraints are then the following:

- $N = N' = 0$:

$$\Sigma(0) \geq 0. \quad (\text{B.7})$$

- $(N, N') = 0, 1$

$$\Sigma(0) \geq 0, \quad \Sigma(1) \geq 0, \quad \Sigma(1) \leq \Sigma(0). \quad (\text{B.8})$$

- $(N, N') = 0, 1, 2$

$$\Sigma(0) \geq 0, \quad \Sigma(1) \geq 0, \quad \Sigma(2) \geq 0, \quad \Sigma(1) \leq \Sigma(0), \quad \Sigma(2) \leq \Sigma(1), \quad \Sigma(0)\Sigma(2) \geq [\Sigma(1)]^2. \quad (\text{B.9})$$

- $(N, N') = 0, 1, 2, 3$

$$\Sigma(0) \geq 0, \quad \Sigma(1) \geq 0, \quad \Sigma(2) \geq 0, \quad \Sigma(3) \geq 0, \quad (\text{B.10})$$

$$\Sigma(1) \leq \Sigma(0), \quad \Sigma(2) \leq \Sigma(1), \quad \Sigma(3) \leq \Sigma(2), \quad (\text{B.11})$$

$$\Sigma(0)\Sigma(2) \geq [\Sigma(1)]^2, \quad \Sigma(1)\Sigma(3) \geq [\Sigma(2)]^2, \quad (\text{B.12})$$

and

$$[\Sigma(0) - \Sigma(1)][\Sigma(2) - \Sigma(3)] \geq [\Sigma(1) - \Sigma(2)]^2. \quad (\text{B.13})$$

LQCD determinations of Mellin Moments should be consistent with these constraints.

References

- [1] E. de Rafael, Phys. Letters **B736** 52 (2014).
- [2] E. de Rafael, Phys. Rev. **D96** 014510 (2017).
- [3] E. de Rafael, *Mellin-Barnes Approach to HVP and $g_\mu - 2$* , invited talk at the First Workshop of the Muon $g - 2$ Theory Initiative, FERMILAB, June 2017.
- [4] G.W. Bennett *et al.* (The $g-2$ Collab.), Phys. Rev. **D73** 072003 (2006).
- [5] Th. Blum, A. Denig, I. Logashenko, E. de Rafael, B. Lee Roberts, Th. Teubner and G. Venanzoni, *The Muon ($g - 2$) Theory Value: Present and Future*, arXiv:1311.2198v1 [hep-ph].
- [6] M. Davier, A. Hoecker, B. Malaescu, and Z. Zhang, Eur. Phys. J. **C71** 1515 (2011).
- [7] K. Hagiwara, R. Liao, A.D. Martin, D. Nomura and T. Teubner, J. Phys **G38** 085003 (2011).
- [8] M. Davier, A. Hoecker, B. Malaescu, and Z. Zhang, Eur. Phys. J. **C77** 827 (2017).
- [9] A. Keshavarzi, D. Nomura, and T. Teubner, arXiv:1802.02995v1 [hep-ph].
- [10] M. Della Morte, B. Jäger, A. Jüttner, and H. Wittig, JHEP 03, 055 (2012).
- [11] F. Burger, X. Feng, G. Hotzel, K. Jansen, M. Petschlies and D.B. Renner, (ETM Collaboration), JHEP **02** 099 (2014).
- [12] B. Chakraborty, C.T.H. Davis, P.G. de Oliveira, J. Koponen, G.P. Lepage and R. van de Water (HPQCD collaboration), Phys. Rev. **D96** 034516 (2017).
- [13] Sz. Borsanyi, Z. Fodor, T. Kawanai, S. Krieg, L. Lellouch, R. Malak, K. Miura, K.K. Szabo, C. Torrero and B. Toth, arXiv:1612.02364v1 [hep-lat].
- [14] M. Della Morte, A. Francis, V. Gulpers, G. Herdoiza, G. von Hippel, H. Horch, B. Jäger, H. B. Meyer, A. Nyffeler, and H. Wittig, arXiv:1710.10072v1 [hep-lat].
- [15] D. Giusti, V. Lubicz, G. Martinelli, F. Sanfilippo, and S. Simula, arXiv:1707.03019v2 [hep-lat].
- [16] Sz. Borsanyi, Z. Fodor, T. Kawanai, S. Krieg, L. Lellouch, R. Malak, K. Miura, K.K. Szabo, C. Torrero and B. Toth, arXiv:1711.04980v1 [hep-lat].
- [17] P. Boyle, V. Gülpers, J. Harrison, A. Jüttner, C. Lehner, A. Portelli, and C. T. Sachrajda, arXiv:1706.05293v1 [hep-lat].
- [18] Ch. Lehner, arXiv:1710.06874v1 [hep-lat].
- [19] B. Chakraborty, C. T. H. Davies, C. DeTar, A. X. El-Khadra, E. Gámiz, S. Gottlieb, D. Hatton, J. Koponen, A. S. Kronfeld, J. Laiho, G. P. Lepage, Y. Liu, P. B. Mackenzie, C. McNeile, E. T. Neil, J. N. Simone, R. Sugar, D. Toussaint, R. S. V. de Water, and A. Vaquero, arXiv:1710.11212v1 [hep-lat].
- [20] G. Abbiendi *et al.*, Eur. Phys. J. **C77** n3 139 (2017).
- [21] B.E. Lautrup, A. Peterman and E. de Rafael, Phys. Rep. **C3** 193 (1972).
- [22] E. de Rafael, Phys. Lett. **B322** 239 (1994).
- [23] T. Blum, Phys. Rev. Lett. **91** 052001 (2003).
- [24] C. Aubin, T. Blum, P. Chau, M. Golterman, S. Peris and C. Tu, Phys. Rev. **D93** 05450 (2016).
- [25] M. Benayoun, P. David, L. DelBuono and F. Jegerlehner, arXiv:1605.04474v1 [hep-ph].

- [26] C. Dominguez, H. Horch, B. Jäger, N.F. Nasrallah, K. Schilcher, H. Spiesberger, and H. Wittig, arXiv:1707.07715v1 [hep-ph].
- [27] J.S. Bell and E. de Rafael, Nucl. Phys. **B11** 611 (1969).
- [28] Ph. Flajolet, X. Gourdon and Ph. Dumas, Theor. Comput., Sci. **144** 3 (1995).
- [29] S. Friot, D. Greynat, and E. de Rafael, Phys. Lett. **B68** 73 (2005).
- [30] J.Ph. Aguilar, D. Greynat and E. de Rafael, Phys. Rev. **D77** 093010 (2008).
- [31] S. Friot and D. Greynat, J. Math. Phys. **53** 023508 (2012).
- [32] B. Berndt, *Ramanujan's Notebooks, Part I*. Springer -Verlag, New York, (1985).
- [33] G.H. Hardy, *Ramanujan. Twelve Lectures on subjects suggested by his life and work*, Chelsea Publishing Company, New York, 3rd ed., (1978).
- [34] Ph. Flajolet, S. Gerhold and B. Salvy, The Electronic Journal of Combinatorics, **11** 2 (2005).
- [35] O.I. Marichev, *Handbuch of Integral Transforms of Higher Transcendental Functions: Theory and Algorithmic Tables*, Wiley, New York, (1983).
- [36] G. Fikioris, IEEE Transactions on Antennas and Propagation, **54** no.12, (2006).
- [37] D. Greynat and S. Peris, Phys. Rev. **D82** 034030 (2010), *erratum* Phys. Rev. **D82** 119907 (2010).
- [38] R.B. Paris and D. Kaminski, “*Asymptotics and Mellin-Barnes integrals*”, Encyclopedia of Mathematics and its applications, Cambridge University Press, (2001).
- [39] M. Passare, A. K. Tsikh and O. N. Zhdanov, “*A multidimensional Jordan residue lemma with an application to Mellin-Barnes integrals*”, Contributions to Complex Analysis and Analytic Geometry, Aspects of Mathematics, vol. **E26**, Vieweg Verlag, Wiesbaden, 233 (1994).
- [40] M. Passare, A. K. Tsikh and A. A. Cheshel, “*Multiple Mellin-Barnes integrals as periods of Calabi-Yau manifolds with several moduli*”, Theor. Math. Phys. **109** 1544 (1997) [Teor. Mat. Fiz. **109N3** 381 (1996)].
- [41] H. Bateman and Erdélyi, **Higher Transcendental Functions, Vol. I**, New York: McGraw-Hill, (1953).
- [42] A.P. Prudnikov, O.I. Marichev and Yu.A. Brychkov **Integrals and Series, Vol.3: More Special Functions**, N.J. Newark: Gordon and Breach (1990).
- [43] G. Källen and A. Sabry, Kgl. Danske Videnskab. Selskab, Mat. Fys. Medd. **29** NÅ° 17 (1955).
- [44] B.E. Lautrup and E. de Rafael, Phys. Rev. **174** 1835 (1968).
- [45] J. Mignaco and E. Remiddi, Nuovo Cim. **60A** 519(1969).